Journal of Materials Science: Materials in Electronics (2020) 31:7286–7314
https://doi.org/10.1007/s10854-020-03338-2

REVIEW

Perspectives of chalcopyrite-based CIGSe thin-film solar cell: a review

G. Regmi[1] · A. Ashok[1] · Parul Chawla[2,3] · Pooja Semalti[2,3] · S. Velumani[1,4] · Shailesh N Sharma[2,3] · H. Castaneda[4]

Received: 20 October 2019 / Accepted: 29 March 2020 / Published online: 10 April 2020
© Springer Science+Business Media, LLC, part of Springer Nature 2020

Abstract
Solar photovoltaic (PV) is empowering, reliable, and ecofriendly technology for harvesting energy which can be assessed from the fact that PV panels with total electricity generation capacity of 505 GW have been installed by the end of 2018. Thin-film solar cells based on copper indium gallium selenide (CIGSe) are promising photovoltaic absorber material owing to an alternative to crystalline silicon (c-Si)-based solar cells because of the huge potential for low-cost solar electricity production with minimal usage of raw materials. The efficiency record of 23.4% was achieved recently in CIGSe solar cells, which was comparable to c-Si solar cells (27.6%). The manufacturing cost of $0.34/W is expected for 15% efficient CIGSe module. The present review article discusses the perspectives of CISe/CIGSe-based thin-film solar cells with the focus on absorber material. Different vacuum and non-vacuum techniques for fabricating these materials are discussed along with the operation of solar cells and their manufacturability. The working mechanism of CIGSe solar cells with the characteristic features of the open-circuit voltage and current density as well as the factors influencing the efficiency in different fabrication techniques are reviewed. Moreover, some strategies toward the improvement of solar cells performance contemplating modified deposition are reviewed. Furthermore, how these strategies can be executed in order to make it cost effective methods is also discussed in detail. Prevailing constrictions for the commercial maturity are deliberated, and future perspectives for improvement at lab as well as industrial scalabilities are outlined.

1 Introduction

Energy is an essential part of techno-socio-economic development all over the world. The improvement in the life expectancy, electrification level, infant mortality rate, mean years of schooling, water access, etc., which are the characteristics of the modern society has a high correlation with the consumption and production of energy [1]. The human civilization has an indication factor for energy harness and its consumption since its inception for the welfare of society. The use of available energy sources enabled humans to improve the quality of life [2]. With the advancement of science and technology for the evolution of energy resources, the subsequence advancement of human society has contributed toward the progressive modern society. The statistics reveal how the quality of life increases with energy consumption, highlighting the importance of energy production, and distribution to an always increasing population [3]. The increase in energy consumption is also related to global population growth. Henceforth, the necessity to enhance the rate of energy production to fulfill the basic requirement needs becomes one of the most challenging tasks that our civilization must face. To balance the energy consumption with its production, different available as well as alternative sources must be explored, which consequently increases the harmful collateral effects. Another aspect of energy balance is the fair distribution of energy that must be taken into insight given many people are still away from the access of basic energy consumption [1–4]. Nowadays, the way the researchers obtain the primary energy is mainly

✉ S. Velumani
velu@cinvestav.mx

✉ Shailesh N Sharma
shailesh@nplindia.org

[1] Department of Electrical Engineering (SEES), Centro de Investigación Y de Estudios Avanzados del IPN (CINVESTAV-IPN), Av. Instituto Politécnico Nacional 2508, Col. San Pedro Zacatenco, CP 07360 Mexico City, Mexico

[2] CSIR-National Physical Laboratory, Dr. K. S. Krishnan Road, New Delhi 110012, India

[3] Academy of Scientific and Innovative Research, CSIR-NPL, New Delhi 110012, India

[4] Department of Materials Science and Engineering, National Corrosion and Materials Reliability Laboratory, Texas A & M University, College Station, TX, USA

through non-renewable sources namely oil, coal, and natural gas which are exhaustible [5], this is because of the reasonably low price for converting fossil fuel to energy. Nevertheless, severe environmental issues are arising out of the use of fossil fuels in the current scenario. The main issue is that fossil fuel, a natural resource of energy, is limited and non-renewable. It underlines the impracticability of the use of fossil fuel energy as if there is an unlimited amount for a much longer time to meet the increasing energy demand. So, it is necessary to remember that, at a certain moment, these resources will start to run out leaving behind not only the hole in energy production but also a high increase of prices which will directly affect the quality of the entire population. Global warming and the emission of greenhouse gas are mainly the cause of the utilization of non-renewable fossil fuels through combustion during energy consumption [6]. Burning of fossil fuels causes emission of long-lived greenhouse gases (GHG), such as CO_2, SO_2, and NO_x, which act to trap heat, radiated from earth's surface, and cause an increase in the surface temperature of the earth. Nowadays, the global warming phenomenon has become a front-page issue since the consequences of increasing earth temperature might cause catastrophic natural disasters, such as inundating, desertification, ice melting, extinction of many species, and deforestation. Different international policy commitments have been adopted for the reduction of greenhouse gas emissions through the reform of our energy consumption and production habitudes based on energy savings and the development of new energy sources [7]. Hence, the dependence on fossil fuels to meet the increased energy demand could have adverse effects on global climatic changes. In this context, the promotion of alternative, environmentally friendly, and renewable energy sources, which generate less or no carbon to the environment, pays much attention as decarbonizing energy is the quickest way to decarbonize the world. Different sources of energy, like hydroelectric, nuclear, and renewables, have been utilized as an alternative source. Renewable energy resources have pivotal importance in the world's future energy sector. To have a scenario of constant growth in population with an equilibrium between factors of high quality of life, the utilization of clean renewable energy sources is necessary as a forward step that humanity must take in the energy production. The most important sources of renewable energy are wind, solar photovoltaic (PV), bioenergy, tidal, geothermal, etc. These energy sources exist virtually everywhere, in contrast to other energy sources, which are concentrated in a limited number of countries. Based on the report of Renewable Energy Policy Network for the twenty-first century, renewable resources shared 20.3% and 26.2% to global energy consumption in 2017 and 2018, respectively. Among these energy consumptions, 15.8% comes from hydropower, 5.5% from wind, 2.4% from solar PV, 2.2% from bio-power, and 0.4% electricity is from the geothermal, concentrated solar power (CSP), and ocean power [8]. The contribution of renewable energy is expected to increase significantly in the upcoming years. Rapid implementation of renewable energy resources can result in remarkable energy security, climate change mitigation, and economic benefits. Besides, renewable energy technology has the potential to lift rural and remote areas, developing countries and underdeveloped to new levels of prosperity. Renewable electricity generation is estimated to increase by 45% during the period 2013–2020, reaching 7310 TWh [8, 9].

Amidst the different renewable energies, solar energy is the most abundant and widely distributed energy source. The sun radiates energy at the rate of 3.8×10^{23} kW, of which 1.8×10^{14} kW is captured by the earth. This indicates that in one second, the sun gives off more energy than people have used since the beginning of the time [8, 10]. Furthermore, solar energy is one of the cleanest sources of energy, creating no harm toward natural resources, such as water, air, and soil. It positively addresses the global warming issue (no emission of greenhouse gases) and does not produce solid or liquid waste materials [11–18]. Other advantages of solar energy that make it as the backbone of serious sustainable development programs include restoration of degraded land, reduction of transmission lines from electricity grids, enhancing the quality of water resources, progress of national energy independence, diversification and security of energy supply, and steady growth of rural electrification in developing countries [19–21]. Hence, it is often referred to as "green energy'' to conventional fossil fuel energy sources.[22, 23]. PV has made magnificent growth in the past decades, and definitely it will play a vital role in global electricity production in the future. Cumulative global PV capacity has increased from 404 GW in 2017 to 505.5 GW in 2018 with more than 100 GW (direct current) of annual installation in 2018 [8]. Thus, 2018 is marked as a record year for the growth of PV capacity.

According to the Shockley--Queisser theory, there are certain requirements for a material to be used as an absorber material in a solar cell [23, 24]. They are as follows: (i) band gap between 1.1 and 1.7 eV, (ii) consisting of readily available, non-toxic materials, (iii) easy, reproducible deposition technique, suitable for large-area production, (iv) good photovoltaic conversion efficiency, (v) long-term stability, (vi) control of conduction type and resistivity, and (vii) high carrier lifetime [25]. The PV market can be divided into different technologies depending on the use of semiconducting absorber material for device fabrication. The bulk crystalline silicon (c-Si)-based solar cells belong to the first generation solar cells which grab the PV market over 90% and have a conversion efficiency of around 27.6% (cell) and 24% (module). Although Si has a near-optimum energy band gap to provide good conversion efficiency being an indirect band

gap material, it has a low absorption coefficient (100 cm^{-1}) which is detrimental from the photovoltaic material point of view. The diffusion length of the photogenerated electrons/holes should be twice the thickness of Si for them to be available at the heterostructure [26]. This will be possible by ensuring a high crystalline quality of Si that demands a complicated manufacturing process and increasing the cost of photovoltaic devices. Thin-film solar cells are expected to grow as new generation solar cells and belong to second generation consisting of amorphous Si (a-Si), cadmium telluride (CdTe), copper zinc tin sulfide (CZTS), gallium arsenide (GaAs), copper indium aluminum selenide (CIASe), and copper indium gallium selenide (CIGSe), which reduce the production cost through the development of new growth and deposition methods of material with few micrometers range of thickness as shown in Table 1. A variety of deposition techniques, including physical, chemical, electrochemical, mechano-chemical, plasma-based, hybrid, can be utilized for growing amorphous to highly oriented films on different substrate configurations. Compositional grading across the thickness of the films can be effortlessly carried out during the growth process even by doping and alloying to obtain high-quality optoelectronic properties [27]. Surface passivation is an important tool to alter the characteristics of the film, which can be performed after the deposition. Furthermore, a flexible thin-film PV module can be installed on the non-rigid and curved surface, which indeed broadens its applicability. The third generation includes dye-sensitized nanocrystalline or Gratzel solar cells, organic polymer-based photovoltaics, multi-band and thermo-photovoltaic solar cells, multi-junction cell, and hot carriers' solar cells, which have emerged to provide higher efficiency while maintaining the low cost offered by second-generation solar cells. The PV electricity needs to be cheaper to take an important share in the energy production for fulfilling the global population's energy needs. The PV market dominated by Si-based solar cells has limitations concerning cost reductions. Silicon is an indirect gap semiconducting material, which is obtained in the form of ingots. Around 200 µm thickness is required for the solar cell application due to indirect band gap nature, homojunction, wafer manufacture complexity, etc. In contrast to Si-based solar cells, CIGSe and CdTe are direct band gap materials with a high optical absorption coefficient allowing to absorb the sunlight completely by 2 µm thickness on rigid as well as flexible substrates [26, 27]. Moreover, the energy payback time (EPBT) of thin-film-based solar cells is 2–3 times lesser than c-Si-based solar cells [28]. The EPBT of thin-film-based solar cell is around 1–1.5 year, revealing the conclusion that the solar cell would contribute to clean usage for more than 23 years, given the assumption of a 25-year operation period. Monolithic integration of thin-film technology allows connecting devices from the front of one cell to the back of the next one in the same plane. Another advantage of a thin film is long-term stability which plays a major factor to achieve commercialization.

Among the thin-film technologies, chalcopyrite-based CISe and CIGSe have been considered promising technologies to facilitate today's PV energy production challenge having the best device conversion efficiency of 23.4% (cells), 17.4% (module) [24, 29]. The CIGSe technology has some competitive characteristics, such as (i) low-cost manufacturing process (vacuum/non-vacuum), (ii) high efficiency on different substrates, (iii) low use of toxic cadmium compared to CdTe, (iv) high radiation tolerance, (v) direct band gap for maximum absorption of photons, and (vi) simplicity for processing steps [30]. In recent years, there has been an immense improvement in efficiency based on an alkali post-deposition treatment. Even higher efficiencies are targeted using tandem solar cells based on thin-film solar cells. Further progress has been made to reduce the thickness of the film by the design of ultrathin solar cells with enhanced properties, which leads to the usage of less materials. In specific, tandem configuration of thin films are considered to dodge the power loss mechanism which occurs in the conventional single-band gap cells due to the incapability to absorb photons beyond the energy band gap and thermalization of photons surpassing their band gap. By the implement of different band gap materials as a stack, tandem configurations are realized with exceeding efficiencies under the Shockley–Queisser theory.

In this article, the perspectives of chalcopyrite-based CISe/CIGSe thin-film solar cells reported in last ten years with the elaboration of different methods for device

Table 1 Physical properties for different thin-film materials [19–24, 26, 27]

Material	Absorption coefficient (cm^{-1})	Band gap (eV)	Toxicity	Sufficient thickness (µm)	Maximum reported efficiency (%)
a-Si	10^6	1.75	None	1	14.0
CdTe	10^6	1.44	Cd	4–5	22.1
CZTS	$> 10^4$	1.5	None	2–3	10.0
CZTSe	$> 10^4$	1–1.5	None	2–3	12.6
CIGSe	$> 10^5$	1–1.7	None	1.5–2	23.4

fabrication and strategies to improve the efficiency and cost by implementing different deposition processes are reviewed. The review has been categorized into different sections which provide some of the important facets of the research area on CISe/CIGSe thin film: (1) theoretical background of thin-film solar cells and its operation; (2) material properties of chalcopyrite-based CISe/CIGSe; (3) state-of-the-art CISe/CIGSe solar cells; (4) review on different deposition techniques to form absorber material; and (5) future perspective and the discussion on the challenges.

2 Theoretical background and operation of solar cells

The solar cell is a photovoltaic device that converts solar energy directly into electricity based on the photogenerated charge carriers in an absorbing semiconductor. The generation of charge carriers by absorption of photons, separation, and collection of those carriers are mainly three steps involved in the operation of solar cells. A semiconducting material always absorbs the photon with energy (E_λ) greater than its band gap (E_g). The absorbed photons excite an electron from the valence band to the conduction band in the absorbing material, i.e., creation of electron–hole pairs (see Fig. 1). The generated charge carrier pairs can either recombine or be separated and then collected (contributing to photogenerated pairs). The number of absorbed photons depends on the thickness and absorption coefficient of the absorber material. The crucial part of a solar cell is the formation of p–n junction, which consists of two semiconductor materials in contact, one n-doped (excess of electrons) and another p-doped (excess of holes) [31]. In a CIGSe-based solar cell, various semiconductor materials are used for the p–n junction formation; hence, the structure is called heterojunction, while in c-Si-based solar cells it is homojunction, i.e., the p–n junction is formed with boron (p side) and phosphorous (n side) doped in the same Si material. The utilization of heterojunction permits the use of a wide-band-gap window layer and hence reduction in surface recombination. The valence and conduction band have discontinuities along with the device structure which can be seen in the energy band diagram of p--n heterojunction (see Fig. 1b). This junction represents the formation possibility of energetic barriers for the charge carrier transport phenomenon. The conversion of minority carriers in p-type absorber layer become majority carriers at the adjacent interface zone by decoupling the physical and electronic junction by the formation of buried junction, hence decreasing the recombination probability [32].

In this study of solar cells by considering a simple single-diode model, where one charge carrier flows the external circuit per each absorber photon, two different currents are considered are follows:

(i) A photocurrent I_{ph} in the reverse direction;
(ii) A forward current I_{dark} corresponding to the diode.

The flow of the current is affected by two resistances: one is series resistance (R_s) and another is shunt resistance (R_{sh}) of the solar cells (see Fig. 2). The total current of an ideal diode (considering series and shunt resistance to be zero and infinity, respectively) can be written as [33]

$$I(V) = I_{dark} + I_{ph}, \tag{1}$$

$$I(V) = I_o\left[\exp\left(\frac{qV}{AKT}\right) - 1\right] - I_{ph}, \tag{2}$$

where I_o is the reverse saturation current of the diode, A is the diode ideality factor, K is the Boltzmann constant, T is

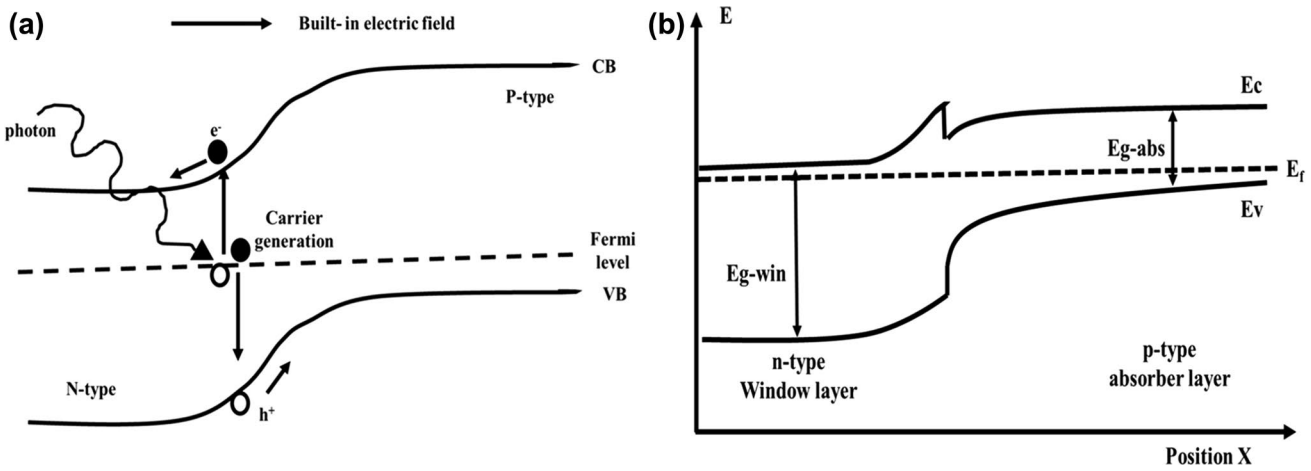

Fig. 1 **a** Schematic diagram of the working principle of a solar cell, **b** energy band diagram of CIGSe-based solar cell

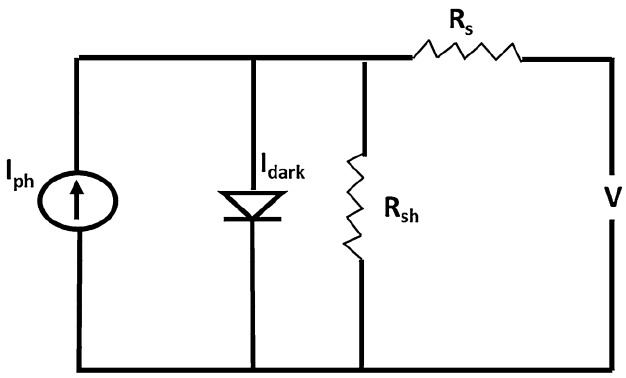

Fig. 2 Equivalent circuit of a thin-film solar cell

the absolute temperature, q is the elementary charge, and V is the applied voltage to the diode.

The current density J in terms of short-circuit current is given by [33]

$$J = -J_{ph} = J_{sc}, \tag{3}$$

where J_{sc} is the short-circuit current density, which is controlled by the current generation and recombination process.

If the flow of current is zero ($J = 0$), then the expression of open-circuit voltage can be written as

$$V_{oc} = \frac{AKT}{q} \ln\left[\left(\frac{J_{ph}}{J_o}\right) + 1\right], \tag{4}$$

where V_{oc} is the open-circuit voltage, controlled by the diode current. Therefore, the relation between J_{sc} and V_{oc} can be written as (ideal condition)

$$J_{sc} = J_o\left[\exp\left(\frac{qV_{ov}}{AKT}\right) - 1\right]. \tag{5}$$

For non-ideal condition ($R_s \neq 0$ and $R_{sh} \neq 0$), the relation between J_{sc} and V_{oc} is given by [33]

$$J(V) = J_o\left[\exp\left(\frac{q(V - R_s)}{AKT}\right) - 1\right] + \frac{V - R_s}{R_{sh}} - J_{ph}. \tag{6}$$

The $Cu(In, Ga)Se_2$ is an I–III–VI_2 semiconductor material, which crystallizes in a tetragonal chalcopyrite structure. The quaternary system Cu–In–Ga–Se is based on the Cu–In–Se and Cu–Ga–Se ternary systems [34, 35]. CIGSe and CGSe have the same crystal structure, except as a matter of fact that some In atoms are superseded by Ga atoms. The chalcopyrite structure of CISe is obtained from the zinc blende structure with the introduction of an additional ordering of the cation sub-lattice, requiring a doubled primitive cell (tetragonal structure) (see Fig. 3) [36]. The structure can be visualized as two interpenetrating face-centered cubic (fcc) lattices: the first anion lattice consisting of group VI atoms (Se^{2-}) and the other being an ordered array of group (Cu^{+}) and (In^{3+}) cations [37]. Each of the Cu or In atoms is bonded tetragonally with four Se anion atoms, whereas each of the Se atoms is coordinated with two Cu and two In atoms. The transition from CISe to CIGSe is achieved by the partial aleatory substitution of indium for gallium atoms. One of the most noticeable effects on the CISe structure with the addition of gallium is the decrease of the lattice parameters. This decrease represents a distortion of the crystal structure and is directly related to the size difference of indium and gallium atoms $\left(\text{atomic radii ratio } {}^{r_{Ga}}/_{r_{In}} \approx {}^{3}/_{4}\right)$. The value of tetragonal distortion is given by $\Delta = 2 - c/a$ and

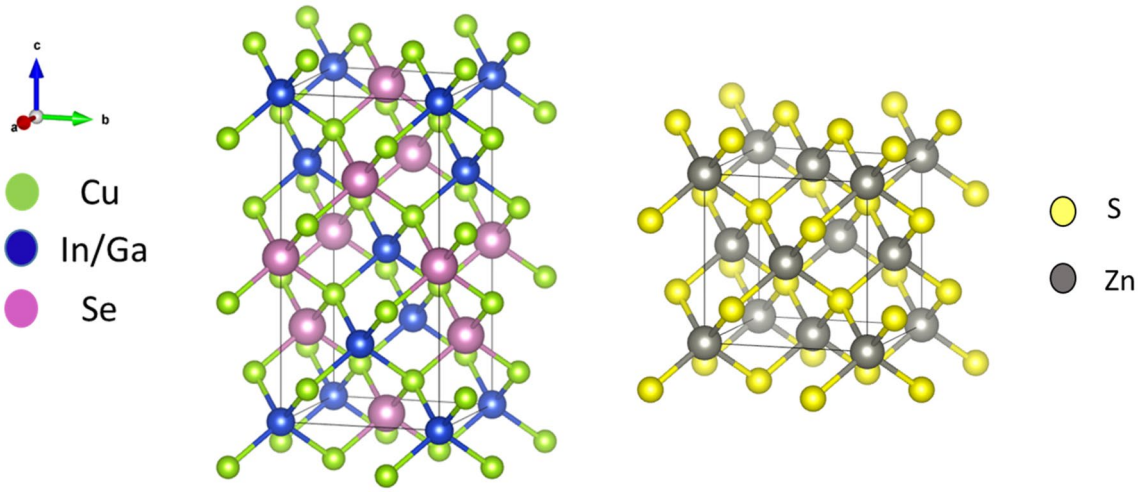

Fig. 3 Unit cell of CIGSe and zinc blende

is depending linearly on Ga content in $Cu(In_{1-x}Ga_x)Se_2$. The value Δ is negative for $x < 0.23$ and positive for $x > 0.23$. It could be due to the change in electronegativities of In and Ga [38–43]. For a pure CISe, the *c*/*a* ratio is close to 2. However, the *c*/*a* ratio deviates toward lower values along with grain refinement due to the substitution of In by Ga atoms. Considering the band structure, the valence band of CIGSe is derived from the weak Cu–Se bond group (I–VI) due to the hybridization of Cu-d and Se-p orbitals. The bottom of the conduction band is mainly contributed from the In and Ga atoms (group III-s orbitals).

The chalcopyrite CISe phase lies on or near the Cu_2Se–In_2Se_3 tie line as shown in Fig. 4. The order defect compound (ODC) phases, such as $CuIn_3Se_5$, $Cu_2In_4Se_7$, and $Cu_3In_5Se_9$, lie on the same tie line. ODC phases are formed due to the regular arrangement of point defects in the chalcopyrite crystal structure [44, 45].

The elementary compositional diagram of CISe varies as a function of formation temperature of different secondary and ternary phases along with Cu_2Se–In_2Se_3 tie line as shown in Fig. 5. According to the phase diagram, there exist α, β, and δ phases of CISe. The desired α-phase of CISe has a chalcopyrite crystal structure, and it exists in a very narrow range of Cu content (24 to 24.5%) at room temperature and higher temperature [46]. On the Cu-rich side, the α-CISe phase exists with the CuSe phase. On the Cu-poor side, CISe exists with β-$CuIn_3Se_5$ ODC phases [47]. A specific defect cluster $2V_{Cu} + In_{Cu}$ (two copper vacancies with indium at copper antisite) also has low formation energy and is responsible for the formation of ODC phases. Moreover, V_{Cu} defect acts as a shallow acceptor. This defect pair has low formation energy and is responsible for the p-type self-doping. On the other hand, Se vacancies (V_{Se}) and In_{Cu} defects act as compensating donors and diminish the p-type conductivity of absorber material. The defects Cu_{In} acts as recombination centers. The δ phase of CISe, which has

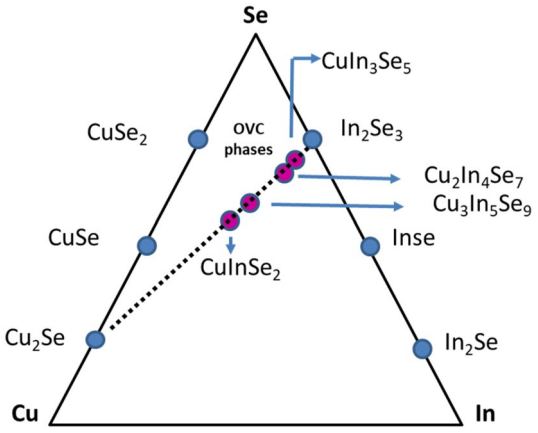

Fig. 4 Ternary elementary compositional diagram of CISe

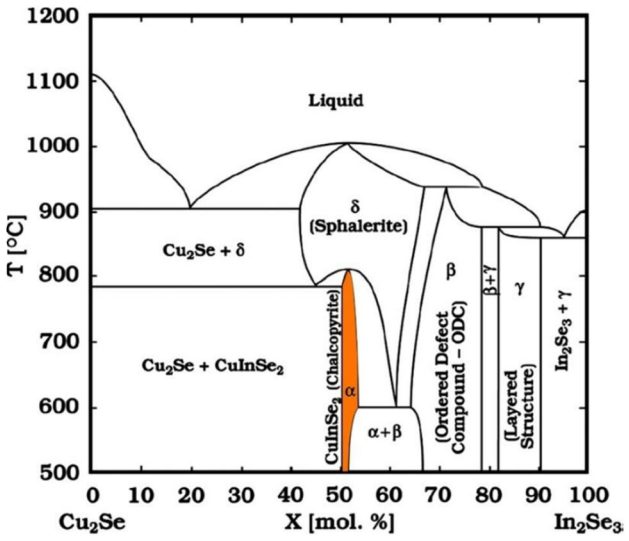

Fig. 5 Pseudo binary Cu_2Se–In_2Se_3 equilibrium phase diagram (reproduced from PhD thesis entitled "Deposition and characterization of $Cu(In_{1-x}Ga_x)Se_2$ films by multiple deposition techniques" presented by Pablo Itzam Reyes Figueroa and supervised by Prof. Velumani Subramaniam and Dr. Nicolas B.) [47]

sphalerite crystal structure exists at high temperature and is unstable at room temperature with a zinc blende unit cell in which metallic cations (Cu^+ and In^{3+}) are randomly distributed. The sphalerite phase differs from the chalcopyrite phase in the random distribution of Cu and In atoms. The introduction of Ga into the CISe system widens the chalcopyrite region toward the lower concentration of Cu content (20.7%). This is believed to be due to the higher formation energy of $V_{Cu} + Ga_{Cu}$ defect pair than $V_{Cu} + In_{Cu}$ pair [44, 48–50]. The stoichiometric composition of CISe absorber material consists of Cu: 25 at.%, In: 25 at.%, and Se: 50 at.%. However, for making p-type material, slightly copper-poor (formation of V_{Cu}) composition is always preferred. Figure 5 shows that the α-CISe phase contains less than 25% Cu, although the α-CISe phase field is very narrow at low temperature and it widens at higher temperature.

3 State-of-the-art CIGSe solar cell

Among the different thin-film solar cell materials, one of the highest efficiency devices have been obtained employing CIGSe absorber layers. The record efficiency for a CIGSe-based solar cell has been recently obtained by Solar Frontier with 23.4% (for a cell area of 1 cm^2) [24]. Before this, for a cell area of 0.5 cm^2, the efficiency of 21.7% was recorded by ZSW, and it was touted for the possibilities for mass production, with ZSW claiming it to be reproducible with achievable efficiencies of over 20% on 40 separate cells in its labs [48].

The state-of-the-art CIGSe solar cell in a substrate configuration is depicted in Fig. 6a, which consists of a multilayered structure of thin-film layers deposited onto the soda--lime glass substrate. Molybdenum (~0.5 μm) as an electrical back contact is generally formed on SLG via DC sputtering. For the p–n junction formation, p-type CIGSe absorber layer and n-type CdS buffer layer are deposited by co-evaporation and chemical bath deposition techniques, respectively. The front contact is formed by a bilayer of i-ZnO and AZO (Al-doped ZnO) with the approximate thicknesses 50–100 nm and 150–200 nm, respectively, as the barrier and conductive layer, deposited by RF sputtering. Ultimately, Nickel–Aluminum (Ni–Al) grids as top metal contacts are deposited onto transparent conducting oxide (TCO) to enhance the charge collection. An anti-reflective (AR) coating onto the full solar cell structure is then evaporated (MgF_2, 105–115 nm) to avoid optical reflection losses. Collectively the top-most 3 layers are hence referred as the "window layer," as the cell is illuminated from ZnO side. The cross-sectional view of the CIGSe-based solar cell structure is depicted in Fig. 6b.

Understanding the contributory roles of each layers in the functioning of solar cell device is crucial factor. The substrate widely used for solar cells (chalcopyrite-based) is soda--lime glass (SLG) as it offers many advantages, such as exhibiting similar coefficient of expansion as CISe in the particular temperature for the growth of the material. The elimination of internal stress can be effected easily by annealing upto 500 °C [51, 52]; SLG itself is a source of sodium to grow chalcopyrite, and its interdiffusion from the glass to absorber improves the grain growth and the solar cell performance by reducing the metal diffusion and supporting the growth of $MoSe_2$ at the back contact [40, 42, 53, 54]. It is also known to dissociate molecular oxygen into atomic oxygen leading to the passivation of Se vacancies. On the other hand, CIGSe formation on borosilicate glass with a lower thermal expansion results in tensile stress (voids and micro-cracks) during cooling process. Similarly, CIGSe formation on a substrate with higher thermal expansion coefficient such as polyimide results in compressive stress which may lead to adhesion failures. SLG has a similar coefficient of thermal expansion (9×10^{-6}/K) as that of CISe/CIGSe, so there are no stress/strain issues. However, for alternate substrates, stress/strain at the interface should be passivated by Na doping (larger grain size, preferred orientation, etc.). Besides, the use of a lightweight and flexible substrates, such as plastic, metal foils, Kapton and Upilex polymeric substrates, at low temperature (<450 °C) for roll-to-roll processing could lower production costs [40, 42].

3.1 Back contact

The preferred back contact is sputtered molybdenum (Mo) owing to its stability under high temperature required for the chalcopyrite deposition [55], and no addition of any n-type doping comes to the picture to recompense p-type doping of CIGSe [56]. Ohmic contact has been established with CIGSe via the formation of an intermediate $MoSe_2$ layer. Lower holes contact resistance (by intermediate layer) helps to reduce the recombination rate. The optimum thickness of Mo is also necessary for the proper functioning as Ohmic contact. For a thick $MoSe_2$ layer, it may induce an excessively high series resistance within the device [54, 57]. Molybdenum Mo, at least for typical cell structures and methods of preparation, seems to be nearly a perfect contact material. However, one of the fewer known issues associated with Mo is its susceptibility to corrosion that reportedly contributes to degradation in the module in accelerated lifetime testing [58]. Poor optical reflection is the other disadvantage of molybdenum, which may become relevant issue to reduce the absorber thickness. It is very thoughtful that the use of Mo-based alloys could enhance stability instead

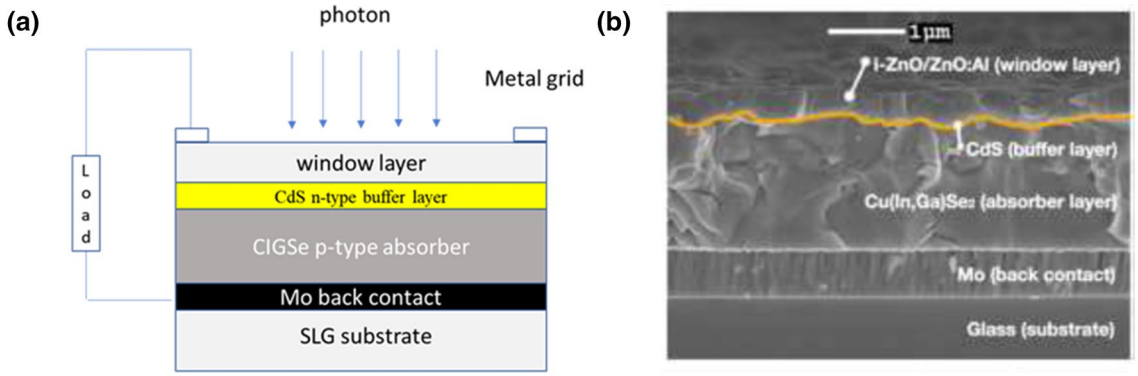

Fig. 6 **a** Standard configuration of a CIGSe solar cell depicting a multilayered structure, **b** Cross-sectional view of CIGSe-based thin-film solar cell (reproduced from PhD thesis entitled "Deposition and characterization of $Cu(In_{1-x}Ga_x)Se_2$ films by multiple deposition techniques" presented by Pablo Itzam Reyes Figueroa and supervised by Prof. Velumani Subramaniam and Dr. Nicolas B.) [47]

of pure Mo. There are various other alternatives for back contact as well, to mention a few: Tungsten appears to yield a good ohmic contact; however, the poor optical properties are one of the main hurdles, while Tantalum and Niobium have slightly higher reflections. Also, preliminary studies indicate the good feasibility in terms of contact performance [50]. TCO-coated metal contacts may become an alternative solution for stability achievement, and good optical as well as electrical performance for solar cells [58–60].

3.2 Buffer layer

Chalcopyrite photovoltaics is formed by the p-type CIGSe absorber layer with a wide-band gap semiconducting n-type window layer. The deposition of an n-type semiconductor window layer (i.e., wide-band-gap material) on the p-type absorber film forms the p–n junction of a solar cell. The window buffer material must have comparatively a larger band gap with respect to the absorber material, which allows the incident photons to reach the absorber layer. Also, the buffer layer has a higher carrier density (around 10^{17} cm^{-3}) compared to the absorber film. In this way, the extension of SCR is wider into the absorber material, thus maximizing the collection of photogenerated carriers. In high-efficiency CIGSe-based solar cells, the buffer layer is a cadmium sulfide (CdS) film deposited by low-cost chemical bath deposition (CBD) method [61–63]. CdS is an n-type semiconductor with a direct band gap value varying from 2.38 to 2.58 eV, having its wurtzite hexagonal (stable, $E_g = 2.58$ eV) or cubic (metastable, $E_g = 2.38$) crystal structure [64–66]. The CdS thin film deposited by chemical bath deposition has a mixed hexagonal/cubic or only hexagonal structure depending on the growth conditions [66]. For high-efficiency CIGSe-based solar cells, a buffer layer with hexagonal structure is preferred over the cubic one, because of its stability and higher optical band gap. Another important parameter for a buffer film is the lattice mismatch with the absorber layer, which impacts the number of interface states. Wada et al. [66] reported a space between planes (d-spacing) of 3.36 Å corresponding to the (111) plane of cubic CdS or (002) plane of hexagonal CdS. The d-spacing of CdS corresponded to the ones related to the (112) plane of CIGSe ($d = 3.34$ Å). It is also observed that those planes of CdS are parallel to the (112) plane of CIGSe. It is important to highlight that the mismatch increases with increasing Ga content [66]. The CdS buffer layer (50–80 nm thick) couples the CIGSe absorber and ZnO window layer in three main aspects: (i) electronically (band alignment), (ii) structurally (lattice match), and (iii) chemically (interdiffusion) [67, 68]. The CdS film grown by CBD participates not only in the formation of the p–n junction but also in the passivation of surface states of CIGSe layer, elimination of surface oxides and protection of the absorber surface from potential damage during the deposition of ZnO window layer [69]. Although many attempts have been carried out to use different CdS growth techniques (e.g., evaporation and sputtering), lower performance has been obtained as compared to CBD [70]. Even though CdS prepared by CBD technique is the best buffer layer for highly efficient CIGSe-based solar cells, it has two main disadvantages: (i) there are concerns about environmental issues and waste disposal because of its toxic nature and (ii) CBD process are not compatible with the in-line vacuum deposition of CIGSe modules. For these reasons, the CIGSe community is trying to replace the CdS buffer layer by different alternative materials, such as In_2S_3 [71] and Zn(OH, S) [72], among others.

3.3 Transparent conducting oxide (TCO)

There are mainly two requirements to be a front contact in chalcopyrite-based thin-film solar cell device: highly transparent in order to allow enough light through the underlying parts of the device, and sufficient conductivity to be able to transport the photogenerated current to the external circuit without dropping too much resistance [35, 58]. Undoped and doped CdS thin film were utilized as a buffer and front contact, respectively, during the early days of CISe and CIGSe solar cell device fabrication [73]. Enough conductivity in doped CdS was obtained by intrinsic doping with Al or In. Spectral losses in conducting CdS were replaced later by TCOs with band gaps of above 3 eV. Various TCOs, such as ITO, SnO_2:F, ZnSe, ZnS, In_2S_3, and ZnO, have been widely used in solar cell fabrication. Nowadays, CIGSe solar cells employ either tin-doped In_2O_3 or, more frequently, RF-sputtered Al-doped ZnO. A transparent conducting ZnO window layer is deposited on top of the buffer layer, which consists of an i-ZnO/ZnO:Al bilayer [74–78]. Al doping in ZnO results in high carrier concentration (in the order of 10^{20} cm^{-3}). TCO, a wide-band gap layer, provides low-resistive contact for the cell [79]. The highly resistive intrinsic zinc oxide (i-ZnO) thin film is deposited directly on the buffer layer (thickness ~ 50 nm) [80]. For the quality improvement of junction and for interface protection from sputter damage while depositing TCO layer, i-ZnO thin layer is deposited [81–83]. Both ZnO layers are deposited by RF sputtering from ceramic targets.

3.4 Ni/Al/Ni grids

Generally, on top of TCO, a current collection grid is fabricated as a metal contact in laboratory test cells. This trio of Ni/Al/Ni is highly conductive and thus minimizes the series resistance of the device [61]. To allow as much maximum light to reach the device, grids should have a minimum shadow area. These grids consist of a stack layer structure with 2 μm in thickness. Firstly, the direct contact of nickel

to the ZnO:Al prevents the oxidation of aluminum present in the window layer. Secondly, the aluminum (Al) layer represents the front ohmic contact of the solar cell. Finally, the second Ni layer avoids oxidation of the Al ohmic contact and allows contacting the top of the grids.

3.5 Na doping

The beneficial effects of Na incorporation could be realized with p-type conductivity improvement due to the increment in hole carrier mobility and open-circuit (V_{oc}) values as well as the intense preferential orientation of prominent (112) reflection plane due to the modification in crystal lattice structure [62, 63, 84]. However, a mechanism for Na acquiring by any of the crystal lattice sites is still unknown, and thus, passivation of grain boundaries is one such explanation which one could predict to have an idea of Na incorporation in CIGSe thin film. Fabrication of CIGSe thin film with simultaneous Na incorporation is a crucial task as sustainment of Na and the further role played till the fabrication of full device structure as well as the film uniformity.

Solution-processed methods in such a questionable scenario for Na incorporation is an approach where the tuning of material along with reduced costs is a boon to explore much in CIGSe. Recently, Colombara and co-workers have explained accidental and deliberate Na doping that occurs all the time during a gas-phase reaction where the vapor pressure of sodium delivery and selenium atmosphere plays a major role and efficiency as high as 8% has been achieved [85]. Incorporating Na to the CIGSe thin film is a complex step and a relatively smaller amount serves as a trigger for obtaining higher efficiency devices. But the question arises that whether the lower/room temperature would favor interdiffusion of Na or the process can only occur at a higher temperature. Another scenario that needs to be discussed is, if a higher temperature is required, would the properties obtained be good enough keeping all the existing elements intact? It has also been reported that the incorporation of Na can take place using the non-vacuum process through in-situ as well as ex-situ mechanisms. An optimum concentration of ~ 1 wt% of Na, for in-situ doping, has been realized, resulting in defect-free formation in device quality CIGSe films which could play a pivotal role in low-cost photovoltaics. In ex-situ doping, annealing as-coated CIGSe on SLG at various temperatures resulted in interdiffusion of Na at a higher temperature of ~ 550 °C. For the same effects realized at a higher temperature in ex-situ doped CIGSe (~ 550 °C), ~ 1% Na-doped CIGSe at a lower temperature (~ 150 °C) proves to be beneficial that could prevent Se effusion at higher temperature. Therefore, the ~ 1% Na-doped CIGSe at ~ 150 °C is an alternative for Mo-coated SLG which can reduce further costs.

3.6 Compositional grading

The state-of-the-art CIGSe thin-film absorber layers are grown by different deposition processes, especially three-stage or multistage co-evaporation, showing a varying [Ga]/([Ga] + [In]) (GGI) ratios across the thickness. The relative elemental composition of Ga determines the band gap energy of CIGSe, which can range from 1.04 eV for pure $CuInSe_2$ to 1.68 eV for pure $CuGaSe_2$, primarily due to a shift in the position of the conduction band maximum [17]. Generally, GGI ratios of around 0.3 are used in record efficiency CIGSe devices which correspond to the average band gap values of approximately 1.15 eV. The concept of the Ga grading profile was first investigated by Contreras et al. and later continued as a three-stage deposition process by co-evaporation [26]. This process leads to better crystallinity of the absorber layer which is based on the interdiffusion of the different metallic precursors and consequently results in the formation of a double grading profile with higher Ga content at the back and the front interfaces, and lower Ga contents in the middle region. The reason behind this is the occurrence of more favorable reaction kinetics between Cu and In than between Cu and Ga. Moreover, this can be explained by the different potential barriers for the diffusion of In and Ga through Cu vacancy defects. As a result, there is strong chemistry between the overall amount of Cu and the shape of Ga grading profile [20]. The formation of grading Ga profile can be influenced by the amount of excess Cu during the second stage of co-evaporation process. Additionally, the formation of the Ga grading can also be affected by other factors such as the presence and amount of alkali metal treatment during the growth of CIGSe thin film, and the deposition parameters (mostly temperature). The elemental grading profile can be controlled precisely by adjusting the growth rate of In and Ga during the deposition of CIGSe thin film. One of the advantages of Ga grading in CIGSe thin film is the presence of a back surface field (BSF) in a gradually decreasing conduction band position, which supports the drift of free electrons toward the front side. This improves the collection of charge carriers at near-infrared region (NIR), as photons having low value of energy are absorbed far from the SCR [25]. Another advantage consists in a front surface grading aiming at a specific alignment of the CBs at the buffer/absorber interface, to prevent a large potential barrier for electrons at the junction and by reaching a small favorable (< 0.3 eV) positive CB offset (CBO) between CdS buffer layer and the CIGSe absorber layer. Besides, the presence of a low band gap region ("notch") close to the front of the absorber for the absorption of low-energy photons. Larger Ga content at the front interface of CIGSe thin film is crucial for improved junction quality in comparison to that in the notch. Jackson et al. reported the improvement in the performance of the CIGSe device from

20. to 21.7% PCE with the engineering of more pronounced front grading [48]. If the amount of Ga is high in the CIGSe film, the notch becomes deep and minority carrier collection from the CIGSe thin film is reduced. The amount of Ga must be varied precisely to obtain a wider band gap > 1.14 eV for high V_{oc} and PCE. However, there are some problems associated with the high band gap CIGSe materials. The cell efficiency decreases due to mid-gap defects/dangling bonds/recombination and band discontinuities at the absorber/buffer interfaces. Moreover, the donor-type defect level is located at 0.8 eV above the valence band edge which affects deep levels associated with donors.

Recrystallization of the CIGSe-based chalcopyrite phase during the co-evaporation process might occur shortly before the segregation of Cu-Se secondary phase on the surface. High-quality Cu-poor films could, therefore, be achieved without reaching a Cu-rich phase [35]. The amount of Cu-excess impacts the position and height of the Ga notch even in two-stage selenization process during the growth of CIGSe thin film. Ga accumulation at the back, near the Mo back contact interface, is undesirable for high-efficiency cells. Therefore, metallic precursor and selenization conditions are optimized for appropriately homogenized Ga profile in two-stage selenization process. Highly efficient CIGSe thin films are typically grown as a slightly Cu-poor material, with [Cu]/([In] + [Ga]) (CGI) ratios of 0.88 to 0.94. CIGSe demonstrates a significant tolerance under stoichiometric amounts of Cu, because of the formation of stable Cu-deficient defect complexes. However, Cu-rich composition shows the better semiconductor properties with improved transport properties and lower defect concentrations. It has also been shown that there should be the phase transition between the Cu-poor and Cu-rich compositions for the stress release during the growth of CIGSe thin film. The reduction in the performance of CIGSe device is mainly due to recombination at or near the interface by limiting the V_{oc} values [46].

4 Deposition methods

Growth conditions of the CIGSe thin film have a critical role in the structural, optical, and electrical properties. Thus, the choice of the growth method, as well as the growth process, is a key factor for the achievement of high-performance PV devices. On the other hand, one of the most important difficulties for thin-film photovoltaic technology to become globally adopted is closely related to the cost of energy produced (cost per Watt). The reduction of this cost could be achieved either by improving conversion efficiencies of solar cells or by the optimization of fabrication processes (e.g., material utilization) or development of new fabrication/deposition methods (e.g., implying the use of low-cost techniques, less pure precursors, and the inclusion of sulfur). Nowadays, the thin-film deposition methods are mainly divided into two groups, namely, non-vacuum and vacuum. Electrochemical [86, 87], nanoparticle (doctor blade and spin coating) [88, 89], and spray-based deposition [90–93] are among the non-vacuum techniques. Amidst the existing vacuum techniques, the co-evaporation [94, 95], sputtering [96], and selenization [97] are the most important ones.

High-efficiency devices are achieved mostly by those techniques performed under vacuum conditions. Co-evaporation of elemental precursors [48, 94] and reactive annealing of precursor films under selenium atmosphere (elemental Se or H_2Se vapor) [98] are the techniques allowing the achievement of highest efficiencies. Although these techniques offer the best performances, they also involve high capital investments in specialized equipment that have issues with the material utilization efficiency (depending on the vacuum deposition technique). In comparison, non-vacuum deposition techniques represent a low production cost through the utilization of low-cost equipment, high material utilization efficiency, and easy scale-up. Nevertheless, solar cells prepared by non-vacuum methods exhibit lower conversion efficiencies in comparison to those achieved with vacuum processes. Considering large-scale productions of CIGSe, a simple example to elucidate one difference between the deposition cost of films with vacuum and non-vacuum methods, rather than the deposition itself, is the storage of the precursor chemicals. On one hand, the storage of Ga trace metals basis (Ga source used in vacuum co-evaporation) must be done at 2–8 °C in low-humidity atmosphere to prevent melting and harmful oxidation of the material. On the other hand, the gallium (III) chloride (Ga source used in non-vacuum chemical spray pyrolysis) could be stored as an aqueous precursor solution at room temperature. Stockpiling of precursors in less controlled environments could represent a reduction in cost. This section gives a brief review of the different thin-film deposition techniques, giving special attention to co-evaporation, sputtering (vacuum), and different non-vacuum deposition techniques. Concerning co-evaporation deposition, the different processes (e.g., Boeing, CURO, CUPRO, 3-stage), as well as the importance of the presence of a copper-rich phase during the formation of CIGSe, will be reviewed.

4.1 Co-evaporation process

The co-evaporation is the most used technique for the deposition of high-quality CIGSe thin film, resulting in the best solar cell efficiencies. In this technique, the vapors of different elemental materials are generated simultaneously from evaporation sources. These vapors condense together to form the absorber layer on a heated substrate at a certain distance from sources. The co-evaporation process consists

of multiple steps (or stages) sequentially linked, each one characterized by fixed evaporation rates of individual elements and a set time. The total flux (i.e., atoms per unit time) of each element depends on its vapor pressure in the source and the temperature of the melting point. The temperature of the melted material controls the evaporation rate (R) of the sources as observed in the approximation:

$$\ln(\boldsymbol{R}) = \boldsymbol{B} + \frac{\boldsymbol{A}}{\boldsymbol{T}_s}, \tag{7}$$

where T_s is the surface temperature; A and B are constants. This equation works in the small interval of evaporation rates used for CIGSe growth. Each evaporation source has A and B constants determined by the measurement of the evaporation rate (quartz crystal monitor) or the thickness of the evaporated film. The arrival rate of the atoms to the substrate mainly depends on the distance from the evaporation source and the shape of the flux beam (Φ). When an evaporated atom reaches the substrate, this could be adsorbed (stick to the substrate) or re-evaporated. The sticking coefficient (S_c) [99] is the ratio between the atoms used in the formation of the CIGSe layer (absorbed) and all the atoms that reach the substrate. In the co-evaporation process of CIGSe, sources containing elemental copper, indium, gallium, and selenium are used. The sticking coefficients of copper, gallium, and indium are close to one. In this case, the deposition rate of each material could be equal to the arrival rate. Furthermore, the sticking coefficient of selenium is lower than that of the other metals (*i.e.,* Cu, In, Ga). For this reason, selenium is evaporated in excess (compared to the necessary to form a stoichiometric CIGSe film) to form an absorber without deficiency of selenium [100–107].

4.1.1 One-step process

One of the most simple co-evaporation processes is the one-stage process (see Fig. 7), proposed by Shafarman et al. CIGSe films fabricated by this method with uniform flux have a columnar grain structure, and efficiencies up to 15.9% have been demonstrated with 650 mV of V_{oc}, 33 mA/cm^2 of J_{sc}, and 74% of FF at 550 °C of substrate temperature. 11.3% of efficiency was reported by the same process processed at 400 °C of substrate temperature with V_{oc} 560 mV, J_{sc} 29 mA/cm^2, and FF 69%. This process consists of the simultaneous evaporation of all elements at fixed evaporation rates at a constant substrate temperature [104]. Evaporation rates are set to nominal values that result in a final composition, i.e., slightly Cu-poor ([Cu]/ ([Ga] + [In]) ≈ 0.85) which has a Ga content of [Ga]/([Ga] + [In]) ≈ 0.35 for the highest solar cell efficiencies. The morphology of the growth layers is distinguished by relatively small (< 1 μm) columnar grains

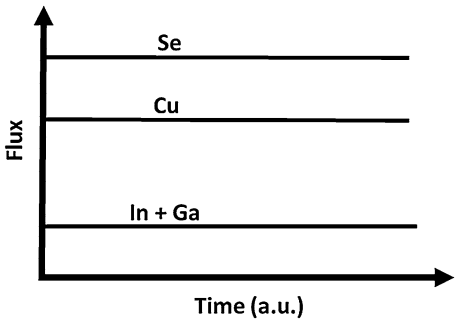

Fig. 7 Schematic diagram of the CIGSe deposition by one-step process

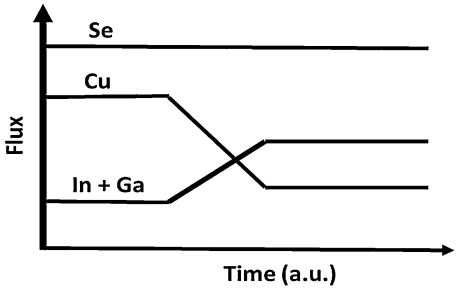

Fig. 8 Schematic diagram of the CIGSe deposition by Boeing process

[103]. The conversion efficiencies of CIGSe devices using the absorbers obtained by this process are around 16% [104].

4.1.2 Bilayer or Boeing process

Bilayer process (see Fig. 8) was first proposed by Mickelsen et al. [101], which is based on two steps:

(i) The first step is the deposition of a copper-rich CIGSe layer ($y > 1$, $y = [Cu]/[In + Ga]$) at relatively low substrate temperature (350 °C—450 °C).
(ii) The second step consists in the decrease of Cu flux along with the increase of indium and gallium fluxes at a high substrate temperature (550 °C—600 °C). This variation in fluxes will lessen the final composition to a sub-stoichiometric in copper ($y < 1$) [107].

Tuttle et al. [105] proposed a growth model of the two-step bilayer process. During the first step ($y > 1$), a separation of CuSe (liquid)–$CuInSe_2$ (solid) phases arise in the form of islands. When the CISe islands coalesce, a thin layer of liquid Cu_xSe ($1 < x < 2$) is formed on the CISe surface. In the second step, the transformation of the "residual" Cu_xSe layer into $CuInSe_2$ is performed with an indium excess (copper flux off) consuming the Cu_xSe phase. The liquid Cu_xSe phase encourages the film growth through a vapor–liquid--solid

mechanism, which progresses the mechanism of diffusion, transport, and reaction kinetics. With this improvement, an epitaxial-like CISe growth is achieved at the liquid–solid interface [105]. The presence of the Cu_xSe phase has an important impact on the observed enhanced grain size (> 1 µm), in comparison to the one-step process (< 1 µm) [101, 105]. Wada et al. [108] proposed another growth model with the formation of a CuSe (liquid)/Cu_2Se (solid) interface. A chemical solid-state reaction takes place from Cu_2Se to CISe through the replacement of copper atoms (in Cu_2Se) by indium atoms diffused through the liquid CuSe phase. Concerning the conversion efficiency of devices, this deposition process allows obtaining around 13% [105].

4.1.3 CURO (Cu-rich/off) process

This process is grounded on the Boeing process, which can be considered as an extreme Boeing co-evaporation process and consists of fixing the substrate temperature along with the indium and gallium fluxes during the whole deposition process. At certain deposition time, the copper flux is stopped in order to obtain a final CIGSe with slightly Cu-poor composition ($y < 1$) (see Fig. 9) [109]. The morphology of the growth layers is formed by columnar grains with sizes of more than 1 µm [39]. The conversion efficiency of devices using absorbers deposited by this process is around 15–16% from the deposition duration shorter than 15 min using a 2-µm-thick film [104, 109].

4.1.4 Inverted process

The growth of absorber layers is based on an inverse Boeing process in which the deposition of a Cu-free (In, $Ga)_2Se_3$ (at low substrate temperature) is followed by the deposition of Cu and Se (at same substrate temperature). Immediately, heat treatment of the film is performed under selenium flux at high substrate temperature (> 500 °C) (see Fig. 10). During this process, the "*y*" ratio does not exceed the value of 1 [102, 110]. The observed grain sizes of the films grown by this deposition process are in the range of 1–2 µm and the reported efficiencies vary from 13 to 17% [48, 110, 111].

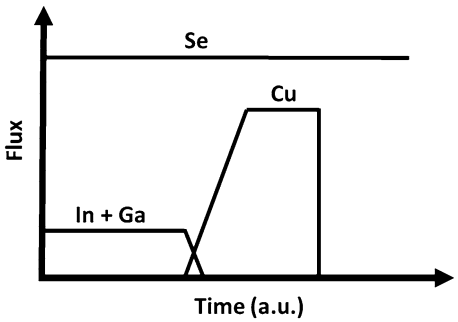

Fig. 10 Schematic diagram of the CIGSe deposition by inverted process

4.1.5 Three-stage process

The CIGSe-based solar cells attain the best conversion efficiencies [112] by the so-called three-stage process which has been optimized in the 1990s as foremost by the National Renewable Energy Laboratory (NREL) (see Fig. 11). This process has the following steps:

- *Step 1* The growth of a 1-µm-thick (In, $Ga)_2Se_3$ thin film is obtained at rather low substrate temperature (250 °C—400 °C).
- *Step 2* The (In, $Ga)_2Se_3$ layers are used as a precursor during the co-evaporation of copper and selenium at high substrate temperature (550 °C—600 °C), where a Cu-rich film is yielded ($y = [Cu]/([In] + [Ga]) > 1$).
- *Step 3* The indium, gallium, and selenium are co-evaporated, and the film evolves gradually to Cu-poor ($y < 1$) until the final composition is reached to nominal scale ($y < 0.9$) [102, 112].

The (In, $Ga)_2Se_3$ is altered via γ-Cu(In, $Ga)_5Se_8$ followed by β-Cu(In, $Ga)_3Se_5$ (both Cu-poor phases) to a final

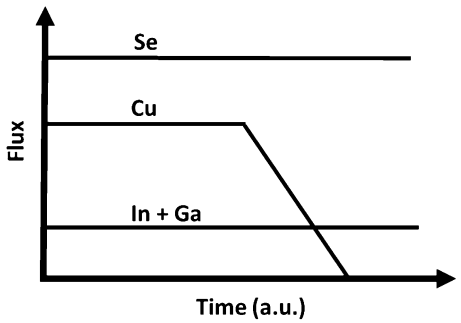

Fig. 9 Schematic diagram of the CIGSe deposition by CURO process

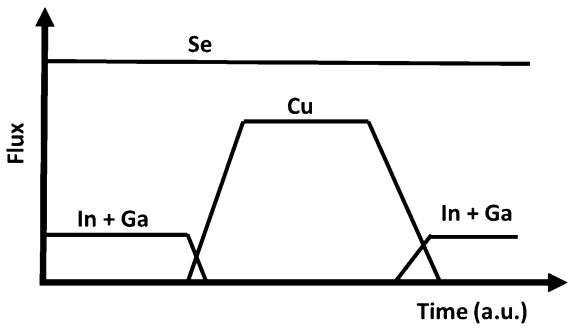

Fig. 11 Schematic diagram of the CIGSe deposition by three-stage process

α-Cu(In, Ga)Se_2. During this alteration process, the Cu_2Se and $(In, Ga)_2Se_3$ materials are brought together to form Cu(In, Ga)Se_2. To accomplish this, a solid-state interdiffusion of In, Ga, and Cu atoms is essential. This diffusion could be carried out via (i) atom–atom replacement, (ii) interstitial migration, or (iii) vacant lattice sites. Among them, the diffusion through vacant lattice sites is the most probable phenomenon [113, 114]. The diffusion rate of copper (diffusion coefficient at 400 °C ~ 10^{-9} cm^2/s) is higher than those of indium and gallium (~ 10^{-13} to 10^{-12} cm^2/s) [113, 115]. Thus, the most probable mechanism for CIGSe formation is the diffusion of Cu atoms into the $(In, Ga)_2Se_3$ along with the corresponding counter diffusion of vacancies into Cu_2Se, which is a characteristic of atomic transport via vacancies [116]. These diffused vacancies gather beyond the solid solubility threshold and promote the formation of voids in the solid [116]. The selenium flux is constant through all the three-stage growth process. Even though each laboratory uses different selenium fluxes, the inclusive purpose is the use of In, Ga, and Se general flux containing an excess of Se. Gabor et al. reported the growth of $(In, Ga)_2Se_3$ films using a [Se]/([In] + [Ga]) flux ratio of approximately 3 [102]. His group also reported the deposition of CIGSe with the use of a [Se]/[Cu] flux ratio of ~ 3 [102]. Mise et al. reported the growth of $(In, Ga)_2Se_3$ with [Se]/([In] + [Ga]) flux ratio of 10 [117]. Although the Se flux is fixed, it has an important role in the deposition process. The Se flux used during the growth of both $(In, Ga)_2Se_3$ and Cu(In, Ga)Se_2 thin films has been reported to affect their morphological, structural, and electrical properties [118–120]. Ishizuka et al. [118] reported the change in surface morphology of $(In, Ga)_2Se_3$ films from triangular to granular grains with the increase in Se flux. One effect of Se flux on CIGSe films is the increase in film porosity with the increase in [Se]/[Cu] flux ratio, probably related to a modification of the Cu–Se phase and the growth dynamics during the third stage of the deposition process [103]. Another effect in CIGSe films is the decrease of hole density with the decrease of Se flux, probably related to the formation of donor-like point defects [118]. Because of all the changes in morphological, structural, and electrical properties of CIGSe films, an impact on the solar cell parameters is also observed, with a substantial change in V_{oc} and FF [119, 120]. More than 22% of photovoltaic conversion efficiency on CIGSe has been achieved by this deposition technique.

4.2 Sequential process

The well-established technology for fabricating the good device grade CIGSe absorber layer for efficient solar cells (> 22%) is a 3-stage co-evaporation process. This technique can achieve high efficiency by the intentional formation of Cu-rich middle layer and a double graded band structure, where the band gap tends to increase toward either side of the middle layer to facilitate high absorption of incident photons and hence separation of photogenerated electrons and hole pairs. However, the high, unwanted cost is associated due to compositional complexity, loss in costly metal sources, the need for an expensive high-vacuum system, etc., for competing to PV market [121]. A potential alternative that can lower the cost of production is a sequential process which is considered as a two-step process, i.e., the deposition of a metallic precursor layer followed by chalcogenization with elemental Se vapor or H_2Se gas. There are various reasons for expecting the lowest production cost: First, the requirement of thermal energy for recrystallization during selenization/sulfurization in a sequential process has a lower thermal budget than the three-stage co-evaporation process [122]. Second, the loss of expensive metal sources, especially In and Ga, can be minimized in a sequential process [123, 124]. Third, the budget for the high-vacuum system is higher in a three-stage co-evaporation process than a sequential deposition process. Moreover, selenization and sulfurization both can be done in a sequential process, but the co-evaporation process only allows selenization. Solar cell manufacturing companies have already demonstrated the high efficiency of up to 22.3% by the sequential process [125]. One of the important reasons for getting lower efficiency from a sequential process is an accumulation of Ga toward the bottom, which lowers V_{oc}. Mitchell and Liu fabricated the CISe/CdS heterojunction solar cell in 1988 with a tremendously high value of J_{sc} of 40.6 mA/cm^2, but the value of V_{oc} was 455 mV, which led to 12.2% efficiency [126]. The insertion of Ga to CISe absorber layer raises the band gap, which enhances the V_{oc}, thereby increasing the efficiency of solar cells despite the loss of long-wavelength absorption of light. The high-efficient CIGSe solar cell generally has a Ga/(In + Ga) ratio of 0.3. Moreover, Ga alleviates the back contact and the absorber layer adhesion by preventing the de-wetting due to the low melting point and high surface mobility of In [127–130].

Sputtering is a widely used deposition technique for the deposition of a metallic precursor layer which is based on the PVD system. This technique has some merits in terms of rate of production and material minimization owing to better growth rate and long life of targets [124]. Generally, the Cu–Ga alloy target is used instead of using Ga and Cu separately to avoid oxidation of Ga. However, In target is used separately to prevent low-temperature Ga–In eutectic reactions [131]. Various stacking approaches to the deposition of different metallic sources have been attempted to improve the efficiency of solar cells. Pinholes can be prevented by Mo/CuGa/In structure resulting from droplets of In; however, this assembly has some malefic results that lead to the lower the efficiency of solar cells [132–135]. The roughness increases while depositing In on the top of the

stack due to the heating effect during selenization that leads to a reduction in shunt resistance. The In droplets formation can be decreased by multiple stacking (In/CuGa/In * *x*) approach of metallic precursor rather than a single-stack (CuGa/In) approach [130]. An investigation has shown that the multiple stack approach led to improved efficiency than bilayer (In/CuGa or CuGa/In) and triple-layer (In/CuGa/In) structure. The roughness of the absorber fabricated from multiple stacks was lower than that of a bilayer and triple-layer structure which lowers the shunt density. Moreover, the wettability of the metal precursor layer can be improved by the multiple stack structure. A single Cu–Ga–In ternary target has been utilized to obtain a metallic precursor layer considering an improvement on the uniformity of film as well as simplifying the process with the attention of nominal composition required for high-efficiency solar cells. In addition to the sequence of metallic precursor layer deposition, the chemical composition of the film highly influences the formation of voids. Ga poor composition favors the formation of In droplets; meantime, Ga-rich composition impedes the rate of reaction for the formation of complete chalcopyrite phase by the establishment of Ga rich γ-$Cu_9(Ga, In)_4$ phase. Compositional changes should be considered during the two-step selenization process, due to high-mobility and favorable Se reaction with Indium, which tend to form Ga-rich phase at the rear surface.

An adhesion issue based on one-pot co-evaporation and the sequential process has compared on solar cells and found that the sequential process had the worst adhesion between Mo and the absorber fabricated on CISe than CIGSe fabricated from the co-evaporation process, probably due to the formation of void at back contact/absorber interface [136, 137]. The thermal expansion of different metals during selenization also causes adhesion problems. Researchers have already investigated to solve the problem of delamination by the incorporation of Ag metal rather than Cu because of having lower melting points of $AgInSe_2$ and $AgGaSe_2$ [138]. Furthermore, the formation of $MoSe_2$ intermediate layer also affects the back contact and the absorber adhesion along with the enhancement of electrical properties of solar cells [139, 140]. The formation of $MoSe_2$ can be influenced by selenization temperature, time, Na supply, quantity of Se, and precursor layer conditions. Another issue of single-stack structure is the formation of In-rich composition at the surface, which degrades the efficiency of the solar cell due to reduced band gap at SCR [141]. Multiple-stack approach favors the lowering of In at surface besides inhibiting the formation of In droplets, which increases V_{oc} [133, 142]. Supply of low Se vapor pressure (by the adjustment of source temperature of Se) and a multiple-stack approach assuage the problem of Ga segregation during selenization because Ga segregation rate is so high under Se vapor condition. A CIGSe thin film fabricated from a Mo/In/CuGa precursor approach has a uniform Ga distribution throughout the entire film with the penalty of pinhole formation compared to the film fabricated from Mo/CuInGa-sputtered single ternary target. So, the combination of very thin Indium layer (80 nm) on the bottom and thin Gallium layer on the surface leads to resolve the problem of pinholes formation by enhancing the V_{oc} and J_{sc} values [143–145]. Ga-rich layer on the bottom side of the film may also lessen the segregation of Ga during the process of selenization, which defines that the total amount of Ga in the precursor layer affects the result of Ga segregation whether to occur or not. The value of V_{oc} and J_{sc} is influenced by the quantity of Ga. Ga inside the SCR impacts the V_{oc}, whereas Ga outside the SCR impacts the J_{sc}, i.e., back grading of Ga should be formed to have a high value of J_{sc}. Wu et al. investigated the effect of Ga-rich layer by varying the thickness near the surface maintaining the constant composition of Ga in the entire metallic precursor layer. The value of V_{oc} was increased while increasing the thickness of Ga near the surface with the penalty of J_{sc}. To have a good efficiency of solar cells, there should be a balance between V_{oc} and J_{sc} [134, 146–150].

The formation of surface stable CISe phase rather than CIGSe phase creates another issue of segregating Ga in the bottom of the film in the sequential process, which pushes out Ga and ultimately causes Ga to diffuse from the surface to the bottom. Segregation of Ga toward the bottom can be minimized by avoiding the formation of selenium vacancy (V_{se}) by the adjustment of Se supply before selenization as the diffusion of Ga occurs during selenization through grain boundaries and V_{se}. Selenium can be supplied to the precursor layer as interlayer which gives the structure of Mo/In/CuIn/Se/CuGa structure [151–153]. Low-temperature pre-heat treatment on pre-deposited Se onto precursor layer before selenization was effective for suppressing the segregation of Ga. The Ga content in the SCR after selenization was 20% when subjected to the pre-heat treatment of 130 °C, but the content of Ga falls to 12% when the pre-heat temperature was 200 °C. It means the segregation process already proceeds during pre-heat treatment. The pre-heat treatment at 130 °C has enhanced efficiency from 5.35 to 8.27%, which was mainly ascribed to the increase in V_{oc} (360–450 mV) from alleviated Ga segregation toward the Mo [134]. The pre-heating approach at 330 °C without the pre-deposition of Se also mitigated the Ga segregation by forming a binary phase, which impedes the formation of CISe chalcopyrite structure responsible for pushing out Ga toward the bottom. Another challenge of the sequential process is the distribution of selenium to the deepest part of the absorber layer. In one-pot co-evaporation process, Se is deposited throughout all the deposition, whereas in a sequential process, Se is supplied to the metallic precursor layer from the surface during selenization so that it is a bit complicated to fed selenium into the deepest part of the absorber layer. To solve the

problem of uniformity to the deepest part the film, Se should be supplied before the crystallization which can be achieved through pure Se or binary compounds (Cu_xSe or InSe). The beneficial effect of InSe phase is to prevent droplet formation of In and leads to the flattening of CIGSe surface. Proper pre-annealing not only allows the sufficient distribution of Se inside the graphite box where a sample is putting but also removes the fine grains of the bottom layer caused by the deficiency of Se, which gives the positive effect, like external quantum efficiency enhancement in long-wavelength range and the decrement in shunt conductance. Accumulated Ga can be infused throughout the entire absorber layer by a proper annealing temperature during the selenization process in the presence of inert gas (see Fig. 12). The final stage of selenization proceeds generally at high temperature (> 500 °C) to obtain a higher crystallinity of CIGSe. Homogenization of Ga should keep in an inert atmosphere instead of under reactive Se because it is thought that V_{se} occurs due to the interdiffusion of Ga and In, because of the higher diffusion rate of Ga and In. The ternary phases, like $CuInSe_2$ and $CuGaSe_2$, should be transformed to single chalcopyrite CIGSe phase by higher recrystallization temperature (in an inert gas atmosphere).

The low value of V_{oc} often results from the sequential process due to the segregation of Ga during the selenization process. Post-sulfurization is a viable way to increase V_{oc} by annealing the CIGSe thin film in the presence of H_2S gas atmosphere, either by evaporating sulfur directly onto CIGSe or by dipping chemically where substitution of Se by S (sulfur) takes place and hence transforming the CIGSe into CIGSSe. This process increases the band gap, increasing V_{oc} maintaining the J_{sc}. Since sulfur atoms are likely to diffuse through the grain boundary from CIGSe surface, it diffuses toward more depth and becomes shallower as the crystallinity and the grain size of CIGSe film increases. It should be remembered to note that the Ga incorporation generally reacts with S and Se reacts with In.

4.3 Non-vacuum Cu(In, Ga)(Se, S)$_2$ formation

The semiconducting material deposited mainly by a non-vacuum process is at low temperature (room temperature to 400 °C) in atmospheric conditions and has advantages of simplicity, low cost, applicable in a large area, and high material utilization efficiency. Non-vacuum methods are divided into three different categories depending upon the scale of mixing starting precursors: (1) particulate-based approach, (2) electrodeposition, and (3) solution-based approach. For large-scale manufacturing, these approaches are attractive due to their effectiveness in large-area deposition, such as ink-jet printing and roll-to-roll processing, in particular, industry-compatible methods [154]. The following discussion will further investigate the different low-cost techniques in detail with their due comparison among themselves to realize the superiority over other methods.

4.3.1 Particulate-based approach

Coating a substrate (flexible, corning glass) with particulate ink offers an efficient method for chalcopyrite thin-film precursor deposition. It requires that the particles should be formed into slurry or ink by dispersal into liquid. This approach constitutes the formation of elemental/precursor submicron powders. The powder obtained is dispersed in a compatible solvent with sonication. The pictorially modeled steps essential for CIGSe film formation have been demonstrated by ZSW [94] (see Fig. 13).

The choice of solvent-cum-capping agent necessitates the consideration of volatility of the solvent used. The sustainment of capping agent during the reaction is crucial for obtaining phase purity in nanocrystals formed. Additionally, it is essential to obtain large-sized nanocrystals for PV applications. It was reported that the formation of single-phase, nearly stoichiometric and mono-dispersive, stable and well-passivated colloidal ternary CISe nanocrystals (band gap (E_g) ~ 1.16 eV) takes place using a novel combination of ligands, viz non-volatile and volatile solvent, 1-octadecene and arylamine aniline, respectively [155]. The synthesis, growth conditions were maneuvered using the colligative properties of the mixture, and thus, higher growth temperature (~ 250 °C) was achieved with the growth of larger grains (see Fig. 14). In a similar report, the mechanism behind attainment of the temperature favored for large-sized nanocrystals has been explained [156]. Considering elevation in boiling point based on vapor pressures of the two solvents used, i.e., aniline and 1-octadecene, the vapor consisted more of aniline in the vapor phase (~ 82%) and 1-octadecene (~ 18%) in liquid phase, contributing to the increment in the boiling point of the mixture [156]. The resulting solutions after successful washing steps are then

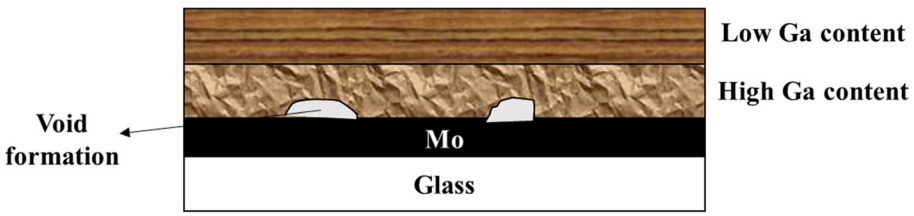

Fig. 12 Growth model mechanism of Ga accumulation and void formation

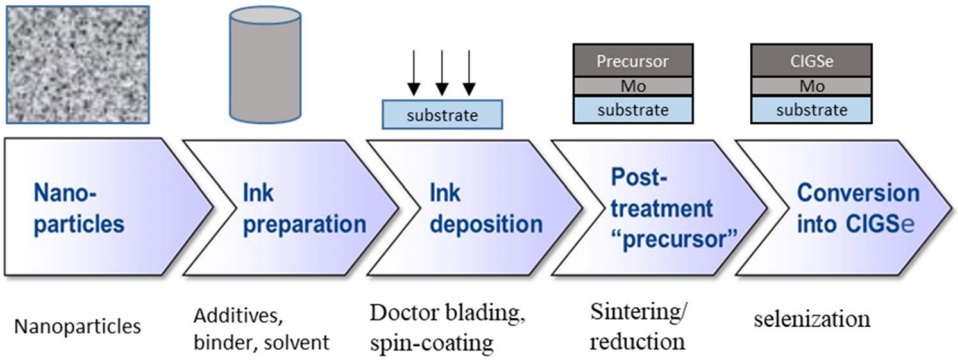

Fig. 13 Schematic diagram demonstrating the coating of a chalcopyrite absorber layer ink; the process explains the dispersion of nanoparticles in a suitable solvent to form an ink-like solution with the addition of binders'/capping agent for stronger adhesion followed by ink deposition using either doctor blade or spin coating technique. Post-deposition treatment is done in Se atmosphere so that the resulting film is not devoid of Se

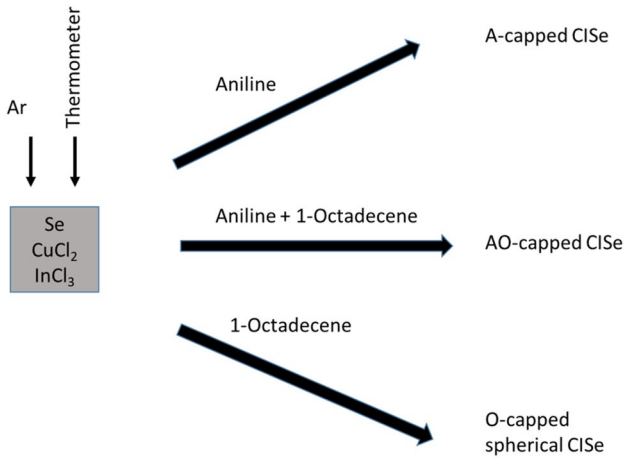

Fig. 14 Schematic diagram depicting the choice of novel ligands and their combination for CISe nanocrystals, wherein combination serves as an effective solvent-cum-agent to obtain phase-pure and large-sized nanocrystals along with the attainment of suitable temperature (~ 250 °C)

deposited onto the substrate for the formation of the absorber layer.

After deposition, the films are subjected to annealing that eliminates the porosity and favors large grain growth, resulting in the formation of a dense film. Synthesis of particles with, phase purity, a well-defined structure and with optimum optical and electrical properties is a crucial task to obtain better film uniformity and in turn the performance of the device [157]. The synthesis of these particles or the nanoparticles is complicated as stoichiometry control with uniform size and composition are the must-have for this method [155, 157].

However, one cannot forsake the layer's porosity while considering other limitations as porous films can lead to shorting of the device and all the efforts in vain. Thus, post-deposition annealing is a mandatory factor that can help overcome the porosity issue. This post-deposition annealing is usually done at higher temperature owing a high melting point for CIGSe that can work in restructuring of bonds, thereby resulting in a dense film with negligible porosity. Particulate-based methods also involve utilization of organic ligands as capping agents as well as imparting stability to the material that even leads to a densification of the material on the substrate as they possess binding abilities and can form molecular structures with intermingled long chains that can bind to each other while coating and further annealing of the films. The organic ligands, such as TOPO, oleylamine, and hexadecylamine, are typically used ligands for the colloidal-based synthesis of CIGSe [158]. The bulky ligands employed are insulating in nature and must be removed to avoid hindrance for charge carriers. To allow carrier transport within the layer, these bulky organic ligands should, therefore, be removed. However, removal of ligands causes cracking up in the film, resulting in porosity. One of the research groups shows the optoelectronic and structural properties of quaternary/ternary (CIGSe/CZTSe/CISe) chalcopyrite nanocrystallites surface-passivated TOPO/TOP ligands and compared their charge transfer characteristic properties in their respective polymer: chalcopyrite nanocomposites by dispersing them in a polymer (3-hexylthiophene). The interaction of the polymer with each of the nanocrystals has been envisaged through the non-ligand exchange without the utilization of toxic ligands, such as pyridine. The charge transfer characteristics show a better charge in CZTSe as compared to CIGSe and CISe owing to high crystallinity in CZTSe (see Fig. 15). However, the weaker binding of TOPO/TOP to nanocrystal surface permitted interaction of nanocrystals to polymer matrix of P_3HT without using any ligand exchange process [159].

Utilization of ternary or quaternary particles solution can provide a greater degree of control as the composition of the

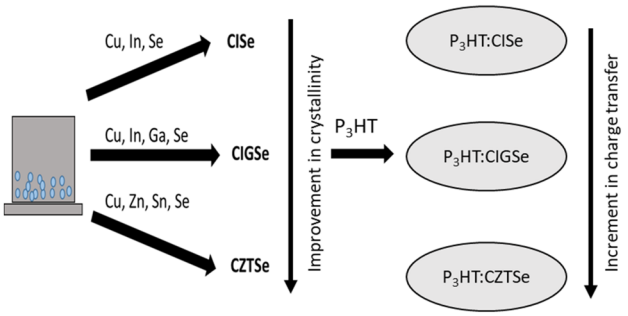

Fig. 15 Schematic diagram demonstrating the mechanism of charge transfer for the ternary (CISe) and quaternary chalcopyrite (CIGSe, CZTSe) in interaction with the regioregular polymer P_3HT. Among the set of chalcogenides, CZTSe has been found to have acquired the most stable stannite/kesterite phase. CZTSe nanocrystals owing to its higher crystallinity show a higher rate of quenching owing to the efficient charge transfer between P_3HT and CZTSe as compared to the corresponding CISe/CIGSe counterparts

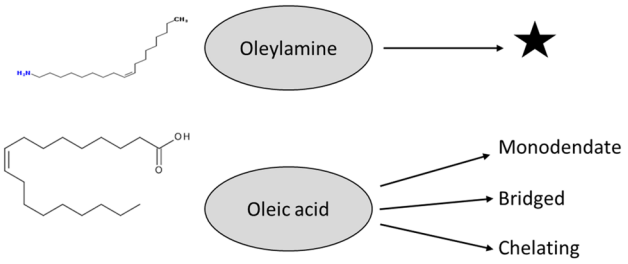

Fig. 16 Illustration of binding modes in oleylamine (OLA) and oleic acid (OA) capping ligands. These ligands show that oleylamine exhibits only one binding mode through lone pair on oxygen, while oleic acid exhibits three different binding modes, viz monodentate, bridged, and chelating. All the three binding modes provide a better orientation of carboxylate anion on nanocrystals surface; thus, CIGSe capped with OA is extremely stable and removal of capping ligand is extremely difficult. However, the combination would bind so strongly with the nanocrystals that interparticle interactions would be almost impossible and hence the charge transport. Using the ligand-exchange process with metal chalcogenide complexes-capped particles could not result in the improvement of properties further

solution can be directly transferred to the substrate [160] with their inhomogeneities on the film with constant stoichiometry. While only CIGSe precursor is used for thin-film fabrication, no additional method is required for the removal of by-products. Researchers at NREL deposited CIGSe by spray pyrolysis followed by selenization [161]. However, this could not result in higher PCE values (only ~ 4.6%) due to the inefficacy of sintering methods to a major extent. Higher efficiency (~ 12.5%), as well as successful fabrication of CIGSe nanoparticles, has been achieved through the utilization of oleylamine (OLA) as a capping agent and alkanethiol, such as dodecanethiol, as a solvent [162]. Additional efforts were also made to substitute OLA with other capping agents as this long-chain amine can hinder the charge transport. It has been reported that the binding capabilities of different ligands, like OLA (oleic acid) and oleylamine + oleic acid, in contrast to TOPO/TOP are different and OLA-capped CIGSe acts as a better capping agent for the synthesis of quaternary CIGSe nanocrystals owing to difference in binding capabilities. This study also unveils the green chemical approach for CIGSe nanocrystals in replacement to highly toxic TOPO/TOP [163, 164]. Slightly weaker binding in amines (due to single mode of attachment) is beneficial for the charge transport properties while strong hindrance if offered by three binding modes in case of oleic acid. The combination of oleylamine and oleic acid together further leads to inefficient charge transport due to the presence of two strong ligands (see Fig. 16) [163–165].

Another particulate-based method is using binary phase particles and then converting them to the ternary or quaternary phase via annealing them in Se vapor [166]. However, films obtained with selenides and metal oxides precursors exhibit voids and micro-cracks due to the presence of O impurities. In comparison, metal particles have led to better film formation, but the tendency of oxidizing in ambient conditions resulted in impurity phase In_2O_3 that was even detected after selenization [167]. The oxides precursor is reduced by H_2/N_2 to form an alloy of metals (Cu, Ga, and In) and followed by selenization process with selenium powder or H_2Se to form complete chalcopyrite absorber material. A modified method by employing mixed oxide nanoparticles followed by two-stage reduction treatment was attempted by the International Solar Electric Technology, Inc. (ISET) (see Fig. 17) and resulted in success with the obtainment of devices exhibiting PCE of 13.6%.[168]. The detrimental factors in this method are the utilization of toxic H_2Se, whose handling is extremely difficult, and the use of aqueous solvent which can lead to early oxidation of the compound formed. Also, for CIGSe, Nano solar was a leader in the development of particle-based techniques, and it utilized an approach involving mixed selenide nanoparticles and a single-step first-stage annealing treatment, thereby resulting a PCE of 17.1% [169, 170].

4.3.2 Electrodeposition

Electrodeposition (ED) is the process of electroreduction of precursor ions onto an electrode/substrate from an appropriate electrolyte by the utilization of electric current or potential between two electrodes (see Fig. 18). Also, it is a good method for nanomaterials and nanocoating of metals, alloy, and semiconductors. The three-electrode system, such as the substrate on which film grows (working electrode), the inert counter electrode (Pt wire/plate), and the reference electrode (SCE or Ag/AgCl) is applied for electrodeposition. The utilization of flexible metal foils as the substrate can be

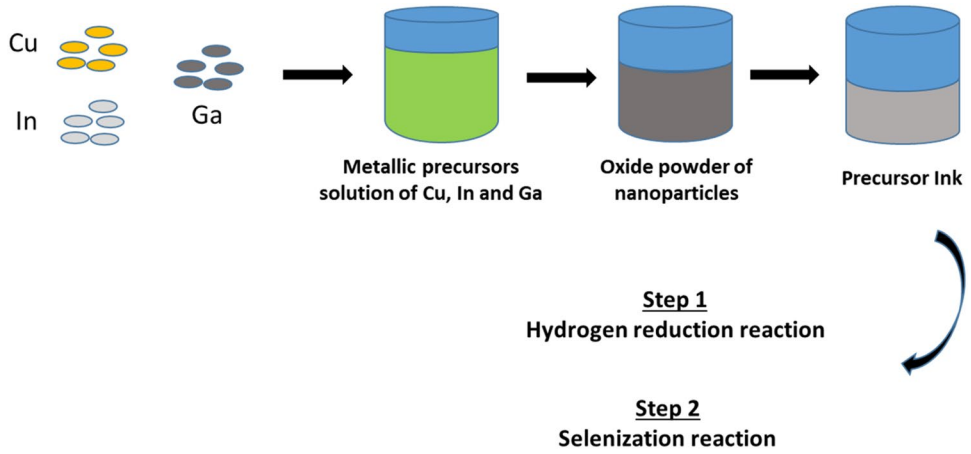

Fig. 17 Schematic representation showing a reduction reaction with ambient hydrogen gas; nanoparticle oxides are converted to a continuous film of alloyed copper, indium, and gallium metals, producing water vapor as a byproduct. Subsequently, the metal alloy film is reacted with H_2Se gas to form high-quality CIGSe thin film

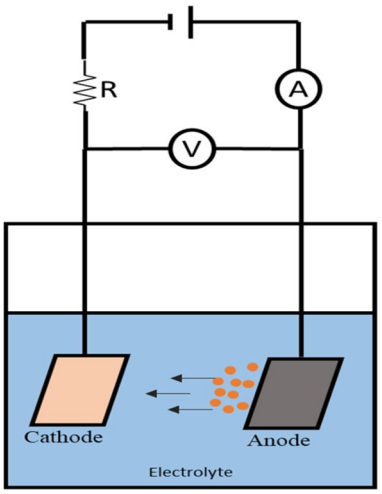

Fig. 18 Schematic diagram of electrodeposition technique

beneficial because the metal foil itself can be used as the working electrode. So that extra layer of material deposition, like Mo, is not necessary for back contact. The properties of the deposited films depend on several parameters, including ionic concentrations, the electrodes used, the pH of the electrolyte, the temperature, the type of substrate, the stirring rate, the deposition voltage, and the time of deposition. Electrodeposition is a promising technology as it allows the deposition of CIGSe thin film cost effectively with no use of expensive vacuum technology and thanks to high deposition rate on larger areas with lateral uniformity [171]. The use of low-cost starting materials, low temperature for deposition, the different substrate on a variety of shapes, effective utilization of precursors with minimum waste generation, controlling deposition parameters, facilitation of extrinsic doping, and band gap engineering are some of the unique features of electrodeposition technique. Owing to these advantages, electrodeposition satisfies all the necessary criteria for the research and development of CIGSe-based solar cells. Table 2 shows the reported CIGSe solar cell efficiency based on electrodeposition technique.

Electrodeposition of CIGSe thin film is possible via a one-step or two-step process. In a simultaneous one-step deposition technique, the electrode potential of all individual elements is closer to each other by adjusting the concentration and pH of the electrolyte used. In the two-step process, stacked-layer structure of metallic precursors can be deposited, followed by a selenization/sulfurization treatment. A one-step deposition is often preferred in comparison to the two-step process as it simplifies the deposition process and reduces harmful emissions. Moreover, electrodeposition involves two fundamental approaches, namely, direct current (DC) ED and pulse ED. A conventional DC electrodeposition based on a constant current or potential which is applied continuously during the growth of materials. DC ED technique effectively has two variables, namely, applied potential/current and time of deposition standing pH of electrolyte and concentration of precursors as a common variable which determines the quality of the deposited material. In this approach, the continuous use of constant potential/current results in the deposition of films without any relaxation leading to the growth of existing nuclei rather than generating new nucleation sites leading to rough and porous film. In pulse electrodeposition (PED), current/potential is applied in the form of sinusoidal waves which offers more controllability of the deposition parameters. The electrochemical deposition has been widely investigated for CIGSe-based deposition since the pioneering work by Bhattacharya et al. in 1983 wherein Cu, In, and Se were simultaneously deposited from an acidic solution [171]. One-step electrodeposition of CISe is usually performed in an aqueous solution often containing chloride/sulfate precursors of Cu^{2+} or Cu^{+}, In^{3+}, and SeO_2/H_2SeO_3. The deposition solution often contains a complexing agent to shift the reduction potentials of Cu and In closer together to improve the film quality. Complexing agents, such as citric acid/citrate, ammonia, triethanolamine, and thiocyanate, are commonly used during

Table 2 Electrodeposited CIGSe-based solar cells with reported efficiency

Absorber material	Preparation method	Reported efficiency	Refs.
CIGSe	Cu/In/Ga oxide precursor followed by thermochemical reduction and selenization treatment	12.4%	[176]
CIGSe & CIGSSe	Four-step electrodepositions of the precursor followed by selenization/sulfurization	15.3% for CIGSe 13.4% for CIGSSe	[206]
CIGSe & CIGSSe	Electrodeposited CIG layers annealed using RTP under S and Se vapors	14.1% for CIGSe 15.8% for CIGSSe	[204]
CIGSe	Electrodeposited CIGSe layers followed by PVD of In, Ga, Se and selenized	15.4% for ED CIGSe 12.4% for EL CIGSe	[174]
CIGSe	Stacked Cu/In/Ga followed by selenization	11.7%	[171]
CIGSSe	Electrodeposition of CIG metal precursors followed by annealing with H_2Se, followed by thermal treatment (Ar) and annealing with H_2S	9.8%	[179]
CIGSe	Stacked Cu/In/Ga by DC and PC electrodeposition methods followed by selenization	11.0%	[173]
CIGSe	Step by step pulse electrodeposition of Cu/In/Ga films followed by selenization	10.4%	[207]
CIGSe	Pulse reverse electrodeposition of CISe followed by selenization	1.4%	[208]
CIGSSe	Electrodeposition of Cu/In/Ga stack followed by thermal treatment at atmospheric pressure with selenium and sulfur	17.3%	[203]

the one-step electrodeposition of CISe thin films. Besides, a supporting electrolyte, such as NaCl, LiCl, and K_2SO_4, is added to improve the conductivity of the electrolyte leading to easier mobility of the precursor ions. There was a necessity annealing the electrodeposited CISe film due to the formation of $Cu_{2-x}Se$ secondary phase which is detrimental to the device performance. Incorporation of Ga into the CISe was a challenging task transforming to quaternary CIGSe compound semiconductor. Bhattacharya et al. reported firstly the inclusion of Ga from a chloride bath with a very low content of Ga/In ≈ 0.1 using 20 kHz of superimposed alternating voltage [172]. But the breakthrough has been realized little later for the incorporation of Ga to CISe using Hydrion buffer (pH 3) consisting of sulfamic acid and potassium hydrogen phthalate with the ratio Ga/In varied from 0.3 to 0.7. CIGSe thin films are generally deposited from one-step electrodeposition technique often used an additional PVD approach to achieve the required composition to form stoichiometric films to be high-efficient solar cells. To overcome the complexity of In and Ga incorporation, alternative strategies have been developed as co-electrodeposition, often involving the deposition of stacked elemental layers, followed by a selenization or sulfurization. Bi et al. successfully utilized the parameters in pulsed electrodeposition to demonstrate CIGSe solar cells with conversion efficiencies up to 10.39% and 11.04%. Cu/In/Ga metallic precursors were electrodeposited by pulse current method wherein the charge density was chosen to achieve the desired thickness of each layer [173].

4.3.2.1 CIGSe-based electrodeposition using an aqueous electrolyte The phenomenon in which electroreduction of ions at a particular reduction potential takes place onto a substrate to form thin films by the effect of an applied electric field in electrodeposition technique. The equilibrium reduction potentials of Cu, In, Ga, and Se ions in the EMF series are + 0.337/SHE, − 0.342/SHE, − 0.529/SHE, and + 0.741/SHE, respectively. The considerably differing potentials often cause the preferential deposition of a single element, and the complex reaction occurs due to the composite electrochemical behavior of selenium, which exhibiting various oxidation states (+6, +4, 0, − 2). Several works on electrodeposition of CIGSe-based absorbers using triethanolamine (TEA) as a complexing agent have been reported after the work from Bhattacharya et al., thereby forming a strong complex with Cu^{2+} and $HSeO^{2-}$ ions and weak complexing with the In^{3+} ions [174]. Liu et al. reported that increasing sodium sulfamate concentration decreases (Cu + Se)/(In + Ga), while gallium content increases and the composition of the CIGSe film transforms from Cu rich to Cu poor [175]. The reduction potential difference between Cu^{2+} and Ga^{3+} was only 80 mV using KCN^- as a complexing agent. Moreover, the reduction of Ga can get catalyzed in the presence of a suitable complexing agent thiocyanate (CNS^-) ions. Duchatelet et al. reported the alternative way for the incorporation of In(III) and Ga(III) in the form of oxides/hydroxides using respective nitrate salts whereby the reduction of In and Ga takes place as two simultaneous mechanisms called nitrate reduction and oxide precipitation [176]. The change in pH of the electrolyte takes place by the consumption of proton during nitrate reduction followed by the deposition of In and Ga in the form of precipitated oxides or hydroxides at very low cathodic potential compared to the electrodeposition of Cu/In/Ga by conventional electrolytes based on sulfates/chlorides. The subsequent H_2 reduction and selenization treatment on electrodeposited CIGSe thin film demonstrated a PCE of 9.4%. Yang et al. reported the controlled introduction of Ga in the form of Ga(III) using

hydrogen peroxide (H_2O_2) as the oxygen precursor [177]. The deposition of In and Ga took place by a controlled mass transfer of the hydroxide species at a relatively higher concentration of H_2O_2 (20 mM). The difficulties encountered in Ga incorporation in conventional Cu/In/Ga electrodeposition can also be easily overcome by the metal oxide/hydroxide approach.

4.3.2.2 CIGSe-based electrodeposition using a non-aqueous electrolyte The formation of pinholes and dendritic morphology due to hydrogen evolution reaction (HER) can be overcome using non-aqueous electrolytes without complexing agents, such as ionic liquids, ethylene glycol, and alcohol/ionic liquid combinations. This approach allows the electrodeposition of In(III) and Ga(III) ions in a more convenient way. Especially, choline chloride (ChCl)-based ionic liquids and aprotic deep eutectic solvents (DES) have selected as an efficient replacement for conventional ionic liquids and volatile organic solvents owing to the advantages, like biocompatibility, non-toxic, cost-effectiveness, and wide electrochemical potential window. In this approach, the high ligand concentrations guarantee more control on the metal speciation in the electrolyte. Steichen et al. reported the electrodeposition of Cu/Ga thin films using reline (a mixture of choline chloride/urea) at 60 °C [178]. The selenized CuGaSe2 PV devices (processed at 550 °C in Se atmosphere) achieved PCE of 4.1%. Malaquias et al. showed the possibility to alter the (Ga/In) ratio from 0 to 1 by modifying the electrolyte flux ratio of (Ga^{3+}/In^{3+}) ions [179].

4.3.2.3 Electrochemical formation mechanism of CIGSe-based absorber layer The formation mechanism of CIGSe-based absorber layer from the electrodeposition technique is complex due to the involvement of electrochemical and chemical reaction that takes place simultaneously. The formation of CuSe binary phase occurs in the first place through underpotential deposition onto the previously reduced Cu from Cu^{2+} ions. The initial formation of Cu is necessary for the direct reduction of Se(IV) to Se(0). The growth of Cu nano-nuclei over Mo-coated substrate permits the inclusion of Se(0) to form Cu_xSe binary phase even at the open-circuit potential. The direct reduction of Se(IV) to elemental Se takes place for increased overpotential. $CuSe_2$ phase could form if the concentration of Se is increased over CuSe which can further reduce to form Cu_2Se at the higher cathodic potential in the presence of H_2Se. Several works of the literature have reported that CuSe phase facilitates the inclusion of In^{3+} ions by the induced co-deposition process when (Se/Cu) ratio is greater than one to form stoichiometric CISe. Excess selenium over CuSe phase is a benefit of the In incorporation at lower cathodic potential during the growth of CISe absorber. Unlike indium, surface-induced reactions of In(III) ions with Cu_xSe phase are not favorable for Ga incorporation to form CIGSe thin film. The introduction of Ga takes place either in the form of $Ga(OH)_3$ (due to the local change in pH) or in the form of Ga_2Se_3 (reaction with H_2Se) at lower or higher cathodic potential, respectively. The incorporation of In and Ga to the growing CIGSe thin film is well suited at a higher cathodic potential. A careful bath preparation and deposition potential are necessary to have controlled inclusion of Ga with minimal oxygen content.

4.3.2.4 Effect of deposition parameters on electrodeposited CIGSe-based absorber layer Good quality of the CIGSe thin film can be achieved by adjusting the deposition parameters in the electrodeposition technique. The use of appropriate additive/supporting chemicals, complexing agents, pH of the electrolyte, deposition potential, bath temperature, etc., determines the quality of CIGSe thin film. The nature of the supporting electrolytes (sodium/lithium-chloride/sulfates) to control the pH and ionic conductivity of the bath influences the quality of the CIGSe film, especially, the morphology. The use of buffering agents, such as sulfamic acid, potassium hydrogen phthalate, and ethylenediamine, helps in bringing the deposition potential of precursors along with the stabilization of the bath. Complexing agent (trisodium citrate) helps in increasing the viscosity of the salt solutions, preventing from oxide formation, enhancing the crystallinity and morphology by reducing the number of cracks, and bringing the reduction potential of Cu, In, and Ga closer to that of Se. Moreover, the composition and the morphology of the film is dependent on the applied potential. CIGSe film with Cu-rich content is known to have larger grain sizes. A Cu-rich composition is preferable if large grain sizes via recrystallization are needed due to active recombination at grain boundaries. Several reports have shown that grain size and grain boundaries of CIGSe layers decrease with increasing Ga contents. The higher annealing temperature helps decrease the roughness by making the grains flat. The interdiffusion of sodium from the substrate helps increase the size of grains and texture at higher annealing temperature which directly enhances the performance of the device. The characteristic features, like the suspension of the freshly deposited metal atoms and the absorption of metal hydroxide, are favored at low pH value. Also, a low value of pH dominates the In deposition. Moreover, it results in hydrogen evolution at a lower cathodic potential. The thickness of the CIGSe thin film was decreased with increasing pH as shown by Rohom et al. They also reported that the electrodeposition potential was found to be shifted toward higher cathodic potential [180].

4.3.2.5 Electroless deposition of CIGSe-based thin film Electroless deposition method is based on short-cir-

cuiting the conducting substrate or a noble metal to an easily oxidizable redox component, like Al or Cd, in the electrolyte bath. To create an electrochemical potential difference between the two electrodes without applying an external voltage, a conducting glass with an easily oxidizable metal is used. This method has the advantage of simplicity as it does not require instrumentation for potentiostatic or galvanostatic control, low-cost process with high deposition rate, and multi-component low-temperature process, and is therefore considered as a promising technology for CIGSe thin-film solar cell fabrication. Bhattacharya et al. reported the co-depositions of Cu/In/Ga/Se by the electroless process from a bath containing 0.02–0.05 M $CuCl_2$, 0.04–0.06 M $InCl_3$, 0.01–0.03 M H_2SeO_3, 0.08–0.1 M $GaCl_3$, and 0.7–1 M LiCl dissolved in deionized water [174]. The films were deposited in a vertical cell in which both working and counter electrodes were suspended from the top of the cell. The combination of both electrochemical and chemical reactions is involved in the electroless process. The deposition potential is composed of the equilibrium reduction potential (E_{eq}), the overpotential, and the ohmic potential drop (iR_s) in the solution. A chemical displacement reaction occurs in this deposition technique, leading to the dissolution of the reactive counter electrode and the reduction of the electroactive species on the substrate.

4.3.2.6 Cyclic volumetric studies on electrodeposited CIGSe The deposition of metal adatoms on a substrate at potentials more positive than that predicted by Nernst equation is known as underpotential deposition. The Nernst equation relates the potential of electrochemical series to the standard potential of a species with the concentrations of analytes in the equilibrium system which can be expressed as follows [181]:

$$E = E^{o} + \frac{RT}{nF} + \ln\left[\frac{O_z}{R_e}\right], \tag{8}$$

where E represents electrochemical cell, E^{o} standard potential of a species, O_z concentrations of the oxidized analytes (O_z), R_e concentrations of reduced analytes, F Faraday's constant, R universal gas constant, n number of electrons, and T represents temperature.

The most important factors determining the formation of electrochemical metal phase on substrate are binding energy between the metal adatoms and substrate, as well as the crystallographic mismatch between them. When the binding energy between the deposited metal adatoms and the atoms of the substrate exceeds that between the atoms of the deposited metal, underpotential deposition takes place. The topic of the underpotential deposition has been studied extensively because the monolayer amount of metal adatoms obtained by this technique alters the electronic properties of the substrate material itself by changing the interfacial activity in terms of fundamental aspects of electrochemical phenomenon. Saji et al. reported the cyclic volumetric studies of unitary, binary, ternary, and quaternary compositions of copper, indium, gallium, and selenium with different concentrations. In the cyclic voltammograms, the first two peaks were copper reduction peaks, the third was the surface oxide's reduction peak, and the fourth corresponded to the hydrogen evolution process. Most of the reported works suggest that a deposition potential in the range of − 0.6 V to − 0.9 V vs standard calomel electrode (SCE) is suitable to achieve a stoichiometric CIGSe film [182]. Kang et al. suggested that the potential below − 1 V is not preferable due to the hydrogen charging [183]. Sang et al. studied the effect of electrodeposition potential on CIGSe thin film by the cyclic voltammetry [184]. It was observed the presence of one weak peak at about 0.15 V, one peak at about − 0.4 V, and one peak at − 0.9 V vs Ag/AgCl. The peak at − 0.9 V was found due to the H^+ reduction to H_2 process. The reduction of In^{3+} to In was observed at − 0.8 V. Similarly, the reduction of Ga^{3+} to Ga was achieved at − 0.9 V from voltammograms of the solution containing $Ga(NO_3)_3$. The underpotential deposition mechanism of Cu/Se and In/Se binary phases was studied in voltammograms of binary and quaternary systems.

4.3.3 Solution-based methods

The solution-based methods firstly involve the ink deposition, followed by annealing. However, this method does not use suspensions and instead utilizes true solutions that restrain the use of additives, and a homogeneous composition is obtained with lesser number of defects [185]. The factors that need to be considered for solution-based methods are solvent's polarity, reactivity, and toxicity [186]. Polar solvents like water are cost effective and environment friendly, but they introduce oxygen impurities in the film, while the non-polar organic solvents lead to the introduction of carbon impurity that deteriorates the device's performance. Precursor elements, their ratios, deposition technique, choice of solvents, etc., are a few of the crucial factors required to be considered on priority before attempting the research.

Solution-based methods involve utilization of any of the following precursors' materials:

(1) Metal salt precursors
(2) Organometallic precursors
(3) Molecular precursors

4.3.3.1 Metal salt precursors Non-vacuum processing of CIGSe involves the utilization of metal salt precursors that directly introduce elements into the solution owing to their

high solubility in a range of solvents [186]. The metal salts have a good solubility mainly in water and alcohol so that the deposition of CIGSe using metal salt precursor solution is considered as the simplest as well as the easiest way. A broad-range technique of deposition can be selected as per the solution viscosity. If the viscosity is low, spraying techniques can be used. If the solution has high viscosity due to the presence of binders, one can use spin coating, doctor blading, etc. Diagrams for these techniques are shown in Fig. 19. In a doctor blading technique depicted in Fig. 19a, a, blade moves over the surface of the substrate, maintaining a proper distance from the surface. The screen printing process (Fig. 19b) demonstrates the utilization of a screen filled with ink. Before the filling of ink, the screen filled by the emulsion that is impervious to the coating ink and some of the open areas allows ink to deposit. Figure 19c shows the spin coating process, i.e., spinning of solution liquid on the surface of the substrate at a high rotational speed. Out of the three methods involved, a spin coating cannot be used to deposit large-area substrates and lead to material wastages.

The doctor blading technique is applied to the deposition of ink precursors over the substrate where binder solution is generally used to adjust the viscosity of the solution [181]. However, binder addition results in the introduction of carbon impurities (in the form of a carbon layer) to the device between CIGSe and Mo back contact [187]. Dissolution of metal nitrates in methanol and addition of ethyl cellulose as a binder was done, and PCE obtained after selenization was 6.7%.[188]. Polymethyl methacrylate (PMMA) was also used as a binder that is known to decompose at low temperature [189]. This resulted in the avoidance of the formation of an intermediate layer, but more inhomogeneities and oxide phase formation were leading to porosity in the film [185]. One of the approaches also performed the coating without binder addition but using an alcoholic solvent and carboxylic chelate complex that results in PCE of 7.7% [190]. However, the method could not prevent the carbon layer formation. The spin coating technique for CIGSe solar cells with the utilization of nitrate salts and PVA as a binder has resulted in cells with PCEs of over 8% [191]. While spraying of CIGSe solution requires low viscosity solutions, the need for binder was eliminated [185].

The deposition of CIGSe thin film by spray pyrolysis method is a simple, cost effective since no vacuum is required, and low-temperature process in relatively larger areas can be coated where pyrolytic small droplets of precursor solution decomposed onto heated substrate. This method involves various steps, such as small droplets of precursor solution, solvent evaporation, solute condensation, the reaction of solute, decomposition, and sintering of films. The atomization of the precursor solution, aerosol transportation, and precursor decomposition on the heated substrate are the main three steps involved in spray pyrolysis. Depending on the atomizer used for the atomization process, spray pyrolysis can be defined into electrostatic, ultrasonic, and air blast (pneumatic) spray pyrolysis. The pneumatic spray pyrolysis equipment consists of the atomizer (nozzle), a substrate heater, carrier gas, temperature controller, and a solution container as shown in Fig. 20. The parameters, such as temperature nozzle-to-substrate distance, the concentration of precursor material, carrier flow rate, pressure time, and types of carrier gas, are most important because film quality can be improved by understanding these parameters.

Normally, metal chlorides or nitrides ($CuCl_2$, $InCl_3$, $GaCl_3$) and thiourea or *N*,*N*-dimethyl selenourea (sulfur and selenium source) are used for the deposition of CIGSe

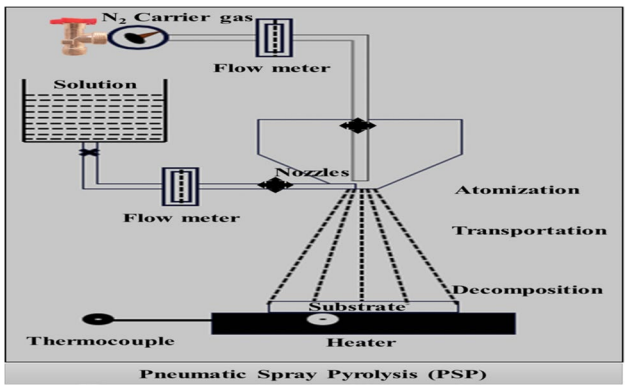

Fig. 20 Schematic diagram of pneumatic spray pyrolysis equipment

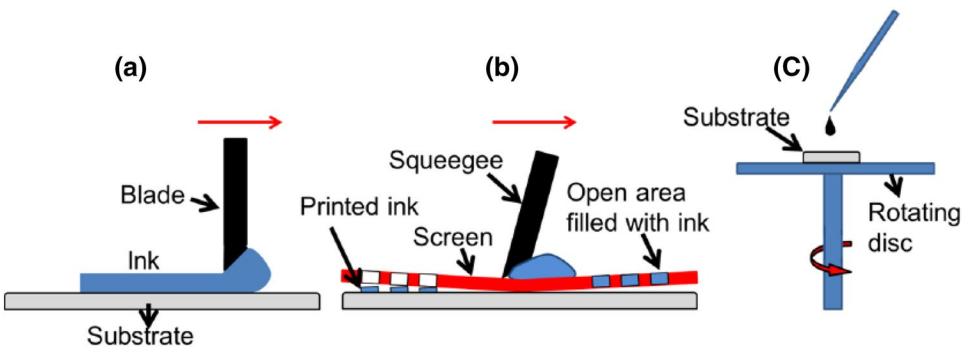

Fig. 19 Schematic diagram of the **(a)** doctor blading, **(b)** screen printing, and **(c)** spin coating techniques

by spray pyrolysis because these precursor materials can easily be dissolved in water and alcohol that helps deposit film nicely. In the spray pyrolysis technique, the precursor is deposited onto the substrate (preheated to ~ 300 to 400 °C), allowing its decomposition. Due to this rapid decomposition, the formation of impurity phases, such as secondary chalcogenides, binary oxides, and by-products like C and Cl, is favored [188]. One cannot choose to have a lower temperature in the spray pyrolysis technique, as the extent of impurities formed is limitless and persists even after further treatment as well [192]. While opting for higher temperature can lead to Se or S effusion, which results in higher porosity in the film. Nevertheless, along-with a temperature range of 300–400 °C, after the deposition annealing is done in Se atmosphere, often required, which results in higher PCEs for sprayed CIGSe. The 10.5% of PCE was obtained by spray depositing the aqueous solutions of thiourea and metal chlorides followed by selenizing the film in a furnace tube [193]. CIGSe-based solar cell with PCE of 10.7% using an aqueous solution of metal nitrates and thiourea with selenization treatment in a glass ampule with Se powder was also reported [194].

4.3.3.2 Organo-metallic precursors Organo-metallic precursors used often for depositing semiconductors using the MOCVD technique with pyrophoric/toxic metal alkyls or hydrides. There could be a variation in thermal reactivity and volatility, and therefore, the composition of product is complicated [195]. Single-source precursor materials have been tried, to overcome these challenges, for ternary $CuInS_2$ and $CuInSe_2$ thin films [196]. The metal–organic molecules are ideal for the growth of CIGSe as they make the process more controllable and the deposition can take place in low-temperature conditions, rendering the material for flexible substrate.

One of the advantages of using a single-source precursor lies in the fact that the method allows for preventing binary phases formation due to the molecular level synthesis [197]. The synthesis of the compound $(PPh_3)_2CuIn\ (SEt)_4$ was reported for the ternary $CuInX_2$ ($X = S$ or Se) semiconductors preparation [192], but the small grain size and the non-uniformity of the as-grown material limit this device performance [197]. An efficiency of 6.7% was obtained when a single-source precursor was used in the PVD method, while only PCE of 1% was obtained by a low-cost non-vacuum technique [198].

4.3.3.3 Molecular precursors The preparation of a soluble molecular complex is the part of this growth approach, via thermally degradable precursors. To convert the precursor into the desired phase, a mild thermal treatment is used which also removes any residual organic species. However, ligands must be wisely chosen for obtaining highly crystalline, crack-free films. The process is generally followed by annealing treatment in a chalcogen atmosphere. Smaller chain ligands are particularly desirable to have smooth film morphology. For example, when hydrazine was used as the solvent, a record PCE for solution deposited CIGSe was obtained. High-quality chalcogenide thin films were obtained by the use of hydrazine, as metal chalcogenides get easily dissolved, such as Cu_2S and In_2Se_3, which are otherwise insoluble in common solvents [199]. The preferred precursors for this method are metal chalcogenides that aid in obtaining high-efficiency devices [200]. Also, hydrazine is a small and volatile material that acts as a strong reducing agent due to its melting point and boiling point temperatures, like water, which are 1.4 °C and 113.5 °C, respectively [196]. Since the single source consists of all the desired elements, a clean step for annealing is enough for final film formation opposed to other CIGSe solution-based deposition techniques [199].

Hydrazine precursors resulting in 12.2% PCE for CISe [197] and 15.2% [186] for CIGSe device fabrication. This methodology, however, is difficult to be implemented in industries since hydrazine is extremely explosive, toxic, and carcinogenic. The approach where processing and handling of precursors is too complicated is not viable for industrial production, and it does not meet up the criteria of cost-effectiveness [199]. To get rid of the issues, there has been active research going on, but a similar approach proposed using alternative solvents, used hydrazine during the step of precursor preparation [201]. Initially, the hydrazinium precursors were prepared by dissolving Cu_2S and In_2Se_3 in hydrazine, dried, and then again dissolved in ethanolamine (EA) and dimethyl sulfoxide (DMSO). But the PCE obtained via this method (3.8%) was limited by small grain size and the lower crystallinity in the films [201].

Pan et al. reported a non-hydrazine molecular-based approach for the deposition of CIGSe, involving a butyl-dithiocarbamic acid-based ethanol solution of metallic oxides. A PCE of 10.1% with high-quality $CuIn(S, Se)_2$ is the result of selenizing these films [202]. Interestingly, most of the work, despite the limitations of this deposition technique, such as wastage of material, is incompatible with roll-to-roll processing, published on molecular-based techniques for CIGSe involves spin coating; hence, other viable alternatives are needed. Spray deposition, which is a high-throughput technique, can make the process much more applicable to large-scale manufacturing.

5 Commercial status

Renewable energy accounted for more than 26% of worldwide electricity generation by the end of 2018. Strong policy and rapid development in new technologies made it possible

contributing one-fourth of global energy generation. Developing and emerging economy strategy has been employed to increase the distribution of renewable energy systems to households in remote areas. The equal contribution goes to the private sector which is playing a key role in driving renewable energy development through its investment and enthusiasm. Global renewable power capacity grew to 2.3 TW in 2018. The annual global market for solar PV slightly exceeded 100 GW for the first time in the year 2018 itself. Evolving market, especially in Europe, compensated for a significant decline in China's PV dominancy resulted from changes in policies, although Asia still overshadowed other regions for fresh installations. Supporting schemes under the policy of government are still needed for solar PV in most countries to drive quickly. China's decision to restrain domestic demand led to global upheaval as Chinese modules inundated the global PV market, and trade gainsays the industrial production in some countries. At least 32 countries had a cumulative capacity of 1 GW or more in solar PV, signifying passionate opinion on renewable energy through the sun.

CIGSe-based solar cell technology has already developed enough to reach industrial-scale production for a commercialization purpose (see Table 3). A fistful of well-established companies is already producing a bulk capacity of CIGSe modules on a glass substrate. These heavy and rigid substrates are mainly used for rooftop and land-mounted installation in utility grid-connected as well as standalone off-grid systems. CIGSe modules are also produced on a flexible substrate like polymer and metal (stainless steel). Apart from rooftop installation and building-integrated PV, CIGSe modules on flexible substrates are used in the transportation system and charging applications. Roll-to-roll processing techniques allow the flexible substrate to enhance production potential as well as a reduction in equipment size for different graded layers. However, so far, standardized roll-to-roll deposition systems are still lagging behind for CIGSe-based solar modules and this is one of the most important reasons why flexible CIGSe modules fall behind their rigid counterparts.

6 Future perspectives and discussion

Various techniques including vacuum as well as non-vacuum approaches for absorber deposition have been demonstrated from R & D to industrial scale. Researcher has shown a rapid progress, and as a result, the reduction in efficiency gap between vacuum and non-vacuum processed CIGSe has been distinguished. Using the hydrazine and particle-based approaches (e.g., Nano solar), the record efficiencies were obtained, implementing viable low-cost technologies [185, 203]. Table 4 shows a summary of the most successful and widely used low-cost deposition approaches to date, indicating the processing steps and challenges.

Non-vacuum methods are typically a sequential process, usually consisting of two steps: (1) precursor deposition step at low-temperature and (2) high-temperature thermal treatment. High-quality material with high crystallinity material is usually obtained after the post-deposition thermal treatment, in the form of clean or reactive annealing (in the presence of S/Se vapor) [185]. The utilization of metal salts is a direct method for CIGSe preparation. For growth technique, methods, such as doctor blade, are used for high-viscosity inks but involve both pre- and post-treatments for removing C impurities (though additives for viscosity adjustment) and selenization, respectively [154]. On the other hand, spray pyrolysis differs in principle from the sequential approaches [185], wherein the solvent is typically evaporated upon contact with or close to the substrate surface and the film growth can take place during the actual deposition step only but typically results in low crystalline films with the presence of more impurities. Certainly, a post-deposition selenization treatment helps improve the material quality, resulting in better PCE [204]. The issues of impurities formation could be avoided in utilizing metal–organic precursors, but composition control makes it difficult to be utilized at a larger scale. Typically, the particle-based approaches require an additional pretreatment to remove the binder/capping and

Table 3 Summary of different methods employed in the non-vacuum process

Precursor type	Deposition technique	Pre-treatment	Post-deposition treatment	Quality of films	Ref
Metal salts	Spray pyrolysis	–	Selenization	Less crystallinity, high content of impurities	[161]
Metal salts	–	–	Selenization	High crystallinity with the presence of impurities	[166]
Metal salts	Doctor blading	Binder reduction	Selenization	Formation of Cu rich film	[187]
Nanoparticles	Printing	Binder reduction	Selenization	High porosity	[158]
Molecular (with hydrazine)	Spin coating	–	Annealing	High crystallinity with less porosity but having high toxicity	[200]
Single-source precursors	Spin coating	–	Selenization	High porosity	[201]

Table 4 CIGSe module manufacturers [209–221]

Company	Substrate	Deposition method	Applications
Ascent solar	Flexible	Co-evaporation	Portable utilities, 10–50 W [209]
Flisom	Flexible	Co-evaporation	Transportation, rooftop installation, portable system application, 25–120 W, 16–17% [210]
Global.solar energy	Flexible	Co-evaporation	Rooftop and transportation installation, portable utilities, 7–300 W, 11–13% [211]
Hanergy-Solibro	Glass	Co-evaporation	Landfill and rooftop installation, 125–150 W, 13–16% [212]
Manz	Glass	Co-evaporation	Rooftop and BIPV installations, 16% [213]
Miasole	Flexible	Sputtering	Chargers, rooftop installations, off-grid lighting system, 12–380 W, 14–17% [214]
Solar Frontier	Glass	Sputtering	Rooftop and landfill installation, 145–175 W, 13–14% [215]
Avansis-CNBM	Glass	Sputtering	Rooftop, landfill and BIPV, 135–150 W, 12–14% [216]
WonCIGS	Glass	Sputtering	Rooftop and landfill installations, 231 W, 16–17% [217]
Stion	Glass	Sputtering	Rooftop and landfill installations, 140–150 W, 13–14% [218]
Midsummer	Flexible	Sputtering	Rooftop installations, portable utilities [219]
HULKet	Glass	Rapid diffusion	Rooftop installations, 100–360 W, 12–15% [220]
Solopower	Flexible	Electrodeposition	Rooftop installations, commercial utilities, 70–260 W, 8–11% [221]

to reduce oxides that might be formed during the process [154]. These additional steps make the technique less cost effective. Nevertheless, employing a ligand where the removal step is avoided would be highly beneficial.

In molecular-based approaches, the hydrazine approach with the use of single-source precursors has the benefit of process simplicity owing to the availability of all the elements at a single step followed by chalcopyrite phase formation due to annealing but has the limitations such as handling and transportation of hydrazine which complicates its use. In addition, the selenization step typically results in poor reproducibility due to the different volatilities of S/Se during selenization [205]. There has been some success in hydrazine-free molecular-based approaches, but complex after-treatment and high-temperature steps are still required [199]. The spin coating has also been involved in these approaches, despite its limitations. An approach combining the benefits of hydrazine-based methods but with less toxic precursors is desirable in order to have better crystallinity in films. Besides, the technique with a minimum number of steps would also aid in obtaining better quality films. Further, the deposition process should also be aimed at high material utilization and potentiality for industrial-scale production.

Challenges faced by non-vacuum-based approaches in terms of fabrication of modules due to processing complexities are otherwise manageable via vacuum methods. The biggest challenge among non-vacuum-based methods is uniformity control with large-area fabrication [222–224]. However, the non-vacuum processes are limited to only absorber layer CIGSe and buffer layer CdS fabrication, while the actual potential of these solar cells could be realized better with the employment of all-solution routes for the complete fabrication. However, working on the absorber layer via non-vacuum methods can still be beneficial in terms of cost-effectiveness and tunability of constituents to get an optimized compound that can offer higher material utilization and no unnecessary wastage of constituents takes place. The other aspect in addition to cost-effectiveness relies upon the increase in PCE values in order to make them a strong competitor with vacuum-deposited CIGSe as well as c-Si. The active research on CIGSe is focused more on cost reduction as well as the obtaining higher PCE values. Different solution-based approaches utilized have yielded equivalent or even better efficiencies than the solar cells fabricated from vacuum techniques.

7 Conclusions

The researchers have reviewed the CIGSe-based semiconductor material properties, operation of solar cells, recent status, and various growth methods used for fabrication. Remarkable progress has been made in the fabrication of highly efficient CIGSe-based solar cells. This paper has also discussed the optical, electronic, and structural properties of copper chalcopyrite materials along with the recent research advances. To obtain high-efficiency CIGSe-based solar cells, the [Ga]/[In + Ga] ratio and [Cu]/[In + Ga] ratio should be around 0.28 and 0.9, respectively. The number of defects in the CIGSe film increases if the Ga ratio exceeds by 0.3. To obtain a high fill factor in CIGSSe solar cells, the [S]/[S + Se] ratio should be less than 0.6. The high-efficiency CIGSe solar cells are produced from Cu-poor absorber because of reduced recombination between CIGSe/CdS heterojunction. The optical band gap of an absorber material should be around 1.15 eV for CIGSe solar cells which can be obtained by the incorporation of Ga into CISe (1.04 eV). Mid-gap defects, recombination at the absorber/buffer heterojunction in a device, get increased as well as the discontinuity in the conduction band becomes cliff. The

overall performance of the CIGSe solar cell improves by a graded band gap profile in the absorber materials. Front grading (close to buffer) improves the V_{oc}, while back grading (close to back electrode) improves the J_{sc} and collection probability. CIGSe solar cells with 23.4% have been reported as champion efficiency via vacuum deposition techniques. A large difference exists between lab-scale (23.4%) and commercial module (17.4%) efficiency due to the difference in growth kinetics over large scale. Besides, various non-vacuum methods, such as particulate ink printing processes and electrodeposition, have reported 17.1% and 17.3% efficient CIGSe-based solar cells, respectively, indicating the maturity of commercial CIGSe module by non-vacuum processes. Non-vacuum solution processes provide high output together with the flexibility of roll-to-roll processing through the investment of low capital compared to expensive vacuum processes. Looking at the cost of materials and scarcity of In, the use of alternative protocol and policy is obligatory. Low-temperature processing and the use of low-thickness (< 1 μm) CIGSe absorbers can be another strategy for effective reduction in manufacturing costs and advancing revenue. Incorporation of alkali after-deposition treatment of absorbers is identified to be pivotal to enhance the efficiency of CIGSe solar cells closer to Shockley--Queisser limit. High-efficiency CIGSe solar cells are mostly fabricated using the CdS buffer layer; however, the trend has changed recently to produce the Cd-free CIGSe module using alternative materials, such as Zn(O, S), (Zn, Mg)O, and In_2S_3. Each component of the CIGSe solar cell structure and its manufacturing art requires further in-depth investigation to simplify the low-cost processing and efficient solar cells. Higher module efficiency, good quality of the absorber layer deposited by alternative/hybrid deposition techniques, optimal composition, and good stoichiometry over large-scale production are some of the major issues related to the development of CIGSe solar cells.

Acknowledgements This work is partially supported by the Project from Consejo Nacional de Ciencia y Tecnología- Secretaría de Energía (CONACyT-SENER)—263043. G. Regmi wishes to thank CONACyT for the doctoral scholarship.

References

1. C. Pasten, J.C. Santamarina, Energy Qual. Life Energy Policy **49**, 468 (2012)
2. Energy Information Administration, International Energy Outlook 2018 (2018). https://www.eia.gov/outlooks/ieo/. Accessed 12 July 2019
3. Energy Information Administration, Annual Energy Outlook 2019 (2019). https://www.eia.gov/outlooks/aeo/. Accessed 12 July 2019
4. International Energy Agency, World Energy Outlook (2019). https://www.iea.org/newsroom/events/publication-world-energy-outlook-2019.html. Accessed 12 July 2019
5. United Nations Development Program, (2018) https://hdr.undp.org/en/content/mean-yearsschooling-adults-years. https://hdr.undp.org/en/content/human-development-index-hdi. Accessed 12 July 2019
6. British Petroleum, BP Statistical Review of World Energy (2019). https://www.bp.com/content/dam/bp/business-sites/en/global/corporate/pdfs/news-and-insights/press-releases/bp-energy-outlook-2019.pdf. Accessed 12 July 2019
7. International Energy Agency, Tracking Clean Energy Progress 2017, 2019. https://www.iea.org/tcep/power/renewables/. Accessed July 12 2019
8. Renewables 2019 Global Status Report, https://www.ren21.net/gsr-2019/. Accessed July 12 2019
9. Intenational Energy Agency, Technology Roadmap Solar Photovoltaic Energy (2019) https://www.iea.org/publications/freepublications/publication/pvroadmap.pdf. Accessed 12 July 2019
10. Fraunhofer Institute for Solar Energy Systems, Levelized cost of electricity renewable energy technologies, (2018). https://www.ise.fraunhofer.de/content/dam/ise/en/documents/publications/studies/EN2018Fraunhofer-ISE_LCOE_Renewable_Energy_Technologies.pdf. Accessed 12 July 2019
11. M.A. Green, K. Emery, Y. Hishikawa, W. Warta, E.D. Dunlop, Prog. Photovolt. Res. Appl. **27**, 3 (2019)
12. B.J. Babu, B. Egaas, S. Velumani, J. Mater. Sci. **29**, 15369 (2018)
13. M. Latha, R.A. Devi, S. Velumani, Opt. Mater. **79**, 450 (2018)
14. A. Ashok, J.S. Narro-Rios, O. Nwakanma, G. Regmi, F.A. Pulgarin-Agudelo, S. Velumani, in *15th International Conference on Electrical Engineering, Computing Science and Automatic Control (CCE), IEEE*, p. 1, (2018)
15. G. Regmi, J.S. Narro-Rios, O. Nwakanma, A. Ashok, F.A. Pulgarin-Agudelo, S. Velumani, in *15th International Conference on Electrical Engineering, Computing Science and Automatic Control (CCE). IEEE*, p. 1, (2018)
16. B.J. Babu, S. Velumani, B.J. Simonds, R.K. Ahrenkiel, A. Kassiba, R. Asomoza, Mater. Sci. Semicond. Process. **37**, 37 (2015)
17. B. Vidhya, S. Velumani, R. Asomoza, J. Nanopart. Res. **13**, 3033 (2011)
18. M. Latha, R.A. Devi, S. Velumani, G. Oza, P. Reyes-Figueroa, M. Rohini, J. Yi, J. Nanosci. Nanotechnol. **15**, 8388 (2015)
19. M. Rohini, P. Reyes, S. Velumani, M. Latha, I. Becerril-Juarez, R. Asomoza, Mater. Sci. Semicond. Process. **37**, 151 (2015)
20. P. Reyes-Figueroa, T. Painchaud, T. Lepetit, S. Harel, L. Arzel, J. Yi, S. Velumani, Thin Solid Film **587**, 112 (2015)
21. B.J. Babu, S. Velumani, A. Kassiba, R. Asomoza, J.A. Chavez-Carvayar, J. Yi, Mater. Chem. Phys. **162**, 59 (2015)
22. M. Chandramohan, S. Velumani, T. Venkatachalam, Mater. Sci. Eng. B **174**, 200 (2010)
23. M. Chandramohan, S. Velumani, T. Venkatachalam, Mater. Sci. Eng. B **174**, 205 (2010)
24. Solar Frontier Achieves World Record Thin-Film Solar Cell Efficiency of 23.35%. https://www.solar-frontier.com/eng/news/2019/0117press.html. Accessed July 28 2019
25. P. Chirila, F. Reinhard, P. Pianezzi, A.R. Bloesch, C. Uhl, L. Fella, D. Kranz, C. Keller, H. Gretener, D. Hagendorfer, R. Jaeger, S. Erni, S. Nishiwaki, S. Buecheler, A.N. Tiwari, Nat. Mater. **12**, 1107 (2013)
26. M.A. Contreras, J. Tuttle, A. Gabor, A. Tennant, K. Ramanathan, S. Asher, A. Franz, J. Keane, L. Wang, R. Noufi, Sol. Energy Mater. Sol. Cells **119**, 296 (2013)
27. S. Hegedus, Prog. Photovolt. Res. Appl. **14**, 393 (2006)
28. P. Reinhard, F. Pianezzi, L. Kranz, S. Nishiwaki, A. Chirila, S. Buecheler, A.N. Tiwari, Prog. Photovolt. Res. Appl. **23**, 281 (2015)
29. Jager-Waldau A, PV status report, 2017. https://publications.jrc.ec.europa.eu/repository/bitstream/JRC108105/kjna28817enn.pdf. Accessed 12 July 2019

30. A. Luque, S. Hegedus, *Handbook of Photovoltaic Science and Engineering*, 1st edn. (Wiley, New York, 2011), pp. 1–41
31. R. Bube, *Photoelectronic Properties of Semiconductors*, 1st edn. (Cambridge University Press, Cambridge, 1992), pp. 60–67
32. H. Mathieu, *Physique des semiconducteurs et des composants électroniques*, 6th edn. (Dunod, New York, 2004), pp. 1–41
33. M.D. Archer, R. Hill, *Clean electricity from photovoltaics*, 2nd edn. (Imperial College Press, New York, 2001), pp. 41–82
34. S.B. Zhang, S.H. Wei, A. Zunger, H. Katayama-Yoshida, Phys. Rev. B **57**, 9642 (1998)
35. W.N. Shafarman, L. Stolt, *Handbook of Photovoltaic Science and Engineering*, 1st edn. (Wiley, New York, 2003), pp. 567–611
36. R. Noufi, R. Axton, C. Herrington, S.K. Deb, Appl. Phys. Lett. **45**, 668 (1984)
37. H. Neumann, R.D. Tomlinson, Solar Cells **28**, 301 (1990)
38. R. Herberholz, U. Rau, H.W. Schock, T. Haalboom, T. Gödecke, F. Ernst, D. Cahen, Eur. Phys. J. Appl. Phys. **6**, 131 (1999)
39. D.J. Schroeder, A. Rockett, J. Appl. Phys. **82**, 4982 (1997)
40. D.W. Niles, K. Ramanathan, F. Hasoon, R. Noufi, B.J. Tielsch, J.E. Fulghum, J. Vac. Sci. Technol. **15**, 3044 (1997)
41. S.H. Wei, S.B. Zhang, A. Zunger, Appl. Phys. Lett. **72**, 3199 (1998)
42. D. Shin, J. Kim, T. Gershon, R. Mankad, M. Hopstaken, S. Guha, B. Shin, Sol. Energy Mater. Sol. Cells **157**, 695 (2016)
43. A. Polman, M. Knight, E.C. Garnett, B. Ehrler, W.C. Sinke, Science **352**, 6283 (2016)
44. M. Kokta, J.R. Carruthers, M. Grasso, H.M. Kasper, B. Tell, J. Electron. Mater. **5**, 69 (1976)
45. Y. Tomm, S. Fiechter, J. Ceram. Process. Res. **6**, 141 (2005)
46. J.C. Mikkelsen, J. Electron. Mater. **10**, 541 (1981)
47. Pablo Itzam Reyes Figueroa, Ph.D. dissertation, CINVETSAV-IPN, Mexico (2016).
48. P. Jackson, D. Hariskos, R. Wuerz, O. Kiowski, A. Bauer, T.M. Friedlmeier, M. Powalla, Phys. Status Solidi RRL **9**, 28 (2015)
49. H. Sugimoto, in *40th IEEE Photovolt. Spec. Conf. (PVSC)*, p. 2767 (2014)
50. J.F. Guillemoles, Thin Solid Films **403**, 405 (2002)
51. F.C. Krebs, Sol. Energy Mater. Sol. Cells **93**, 394 (2009)
52. N.G. Dhere, Sol. Energy Mater. Sol. Cells **90**, 2181 (2006)
53. U. Rau, H.W. Schock, Appl. Phys. A **69**, 131 (1999)
54. X. Zhu, Z. Zhou, Y. Wang, L. Zhang, A. Li, F. Huang, Sol. Energy Mater. Sol. Cells **101**, 57 (2012)
55. O. Nwakanma, P. Reyes, S. Velumani, J. Mater. Sci. **29**, 15671 (2018)
56. A. Krasnov, US Pat., US 9419151 B2 (2016)
57. M. Powalla, B. Dimmler, Thin Solid Films **361**, 540 (2000)
58. Z.J. Li Kao, N. Naghavi, F. Erfurth, J.F. Guillemoles, I. Gérard, A. Etcheberry, D. Lincot, Prog. Photovolt. Res. Appl. **20**, 582 (2012)
59. K. Orgassa, H.W. Schock, J.H. Werner, Thin Solid Films **431**, 387 (2003)
60. K.L. Chopra, P.D. Paulson, V. Dutta, Prog. Photovolt. Res. Appl. **12**, 69 (2004)
61. M. Bär, U. Bloeck, H.J. Muffler, M.C. Lux-Steiner, C.H. Fischer, M. Giersig, F. Karg, J. Appl. Phys. **97**, 014905 (2005)
62. K. Masuko, M. Shigematsu, T. Hashiguchi, D. Fujishima, M. Kai, N. Yoshimura, T. Yamanishi, IEEE J. Photovolt. **4**, 1433 (2014)
63. M.A. Green, K. Emery, Y. Hishikawa, W. Warta, E.D. Dunlop, Prog. Photovolt. Res. Appl. **23**, 1 (2015)
64. P. Reyes, S. Velumani, Mater. Sci. Eng. B **177**, 1452 (2012)
65. M. Cardona, M. Weinstein, G.A. Wolff, Phys. Rev. **140**, A633 (1965)
66. T. Wada, Sol. Energy Mater. Sol. Cells. **49**, 249 (1997)
67. R. Hunger, M.V. Lebedev, K. Sakurai, T. Schulmeyer, T. Mayer, A. Klein, S. Niki, W. Jaegermann, Thin Solid Films **515**, 6112 (2007)
68. C. Heske, D. Eich, R. Fink, E. Umbach, T. van Buuren, C. Bostedt, L.J. Terminello, S. Kakar, M.M. Grush, T.A. Callcott, F.J. Himpsel, D.L. Ederer, R.C.C. Perera, W. Riedl, F. Karg, Appl. Phys. Lett. **74**, 1451 (1999)
69. J. Kessler, M. Velthaus, M. Ruckh, R. Laichinger, H.W. Schock, D. Lincot, R. Ortega, J. Vedel, in *6th Int. Photovolt. Sci. Eng. Conf.*, p. 1005 (1992)
70. M. Rusu, T. Glatzel, C.A. Kaufmann, A. Neisser, S. Siebentritt, S. Sadewasser, T. Schedel-Niedrig, M.C. Lux-Steiner, in *MRS Proc. 865 F14.25* (2005)
71. J. Sterner, J. Malmstrom, L. Stolt, J. Malmström, L. Stolt, Prog. Photovolt. Res. Appl. **13**, 179 (2005)
72. C. Platzer-Bjorkman, J. Kessler, L. Stolt, in *3rd World Conf. Photovolt. Energy Convers*, p. 461 (2003)
73. A. Rothwarf, I.E.E.E. Trans, Electron Dev. **29**, 1513 (1982)
74. Kessler, M. Ruckh, D. Hariskos, U. Ruhle, R. Menner, H.W. Schock, in *23rd IEEE Photovolt. Spec. Conf. (PVSC)*, p. 447 (1993)
75. A. Nelson, A. Gabor, M. Contreras, A. Mason, P. Asoka-kumar, K. Lynn, Sol. Energy Mater. Sol. Cells **41**, 315 (1996)
76. G. Regmi, M. Rohini, P. Reyes-Figueroa, A. Maldonado, M. de la Luz Olvera, S. Velumani, J. Mater. Sci. **29**, 15682 (2018)
77. H. Park, S.Q. Hussain, S. Velumani, A.H.T. Le, S. Ahn, S. Kim, J. Yi, Mater. Sci. Semicond. Process. **37**, 29 (2015)
78. B.J. Babu, A. Maldonado, S. Velumani, R. Asomoza, Mater. Sci. Eng. B **174**, 3 (2010)
79. N. Romeo, A. Bosio, V. Canevari, in *Proceedings of the 8th Eur. Photovolt. Sol. Energy Conf.*, p. 1092 (1988)
80. S.H. Kwon, S.C. Park, B.T. Ahn, K.H. Yoon, J. Song, Sol. Energy **64**, 55 (1998)
81. T. Negami, Y. Hashimoto, S. Nishiwaki, Sol. Energy Mater. Sol. Cells **67**, 331 (2001)
82. T. Negami, T. Satoh, Y. Hashimoto, S. Shimakawa, S. Hayashi, M. Muro, H. Inoue, M. Kitagawa, Thin Solid Films **403**, 197 (2002)
83. M. Romeo, D. Terheggen, D. Abou-Ras, D.L. Batzner, F.J. Haug, M. Kalin, D. Rudmann, A.N. Tiwari, Prog. Photovolt. Res. Appl. **12**, 93 (2004)
84. W. Hoffmann, T. Pellkofer, Thin Solid Films **520**, 4094 (2012)
85. D. Colombara, U. Berner, A. Ciccioli, J.C. Malaquias, T. Bertram, A. Crossay, G. Gigli, Sci. Rep. **7**, 43266 (2017)
86. D. Lincot, J.F. Guillemoles, S. Taunier, D. Guimard, J. Sicx-Kurdi, A. Chaumont, O. Roussel, O. Ramdani, C. Hubert, J.P. Fauvarque, N. Bodereau, L. Parissi, P. Panheleux, P. Fanouillere, N. Naghavi, P.P. Grand, M. Benfarah, P. Mogensen, O. Kerrec, Sol. Energy **77**, 725 (2004)
87. D. Lincot, Thin Solid Films **487**, 40 (2005)
88. M. Kaelin, D. Rudmann, F. Kurdesau, H. Zogg, T. Meyer, A.N. Tiwari, Thin Solid Films **480**, 486 (2005)
89. W. Wang, S.Y. Han, S.J. Sung, D.H. Kim, C.H. Chang, Phys. Chem. Chem. Phys. **14**, 11154 (2012)
90. B. Pamplin, R.S. Feigelson, Thin Solid Films **60**, 141 (1979)
91. M.S. Tomar, F.J. Garcia, Thin Solid Films **90**, 419 (1982)
92. C.R. Abernathy, C.W. Bates, A. Anani, B. Haba, G. Smestad, Appl. Phys. Lett. **45**, 890 (1984)
93. S. Duchemin, J. Bougnot, A. El Ghzizal, K. Belghit, in *Eur. Photovolt. Sol. Energy Conf.*, p. 476 (1989)
94. P. Jackson, D. Hariskos, R. Wuerz, O. Kiowski, A. Bauer, T.M. Friedlmeier, M. Powalla, Phys. Status Solidi RRL **9**, 28 (2014)
95. B. Dimmler, R. Wächter, Thin Solid Films **515**, 5973 (2007)
96. J.H. Shi, Z.Q. Li, D.W. Zhang, Q.Q. Liu, Z.Z. Sun, S.M. Huang, Prog. Photovolt. Res. Appl. **19**, 160 (2011)
97. Y. Tanaka, N. Akema, T. Morishita, D. Okumura, K. Kushiya, in *17th EC Photovolt. Sol. Energy Conf.*, p. 989 (2001)
98. S. Aksu, S. Pethe, A. Kleiman-Shwarsctein, S. Kundu, M. Pinarbasi, in *38th IEEE Photovolt. Spec. Conf. (PVSC)*, p. 3092 (2012)

99. T. King-Ning, J.W. Mayer, L.C. Feldman, Electronic Thin Film Science: For Electrical Engineering and Materials Scientist (1996)
100. NREL, Research cells efficiencies records, (2015). https://www.nrel.gov/ncpv/. Accessed 26 Jun 2019
101. R.A. Mickelsen, W.S. Chen, Appl. Phys. Lett. **36**, 371 (1980)
102. A.M. Gabor, J.R. Tuttle, D.S. Albin, M.A. Contreras, R. Noufi, A.M. Hermann, Appl. Phys. Lett. **65**, 198 (1994)
103. J. Kessler, C. Chityuttakan, J. Lu, J.L. Schöldström Stolt, Prog. Photovolt. Res. Appl. **11**, 319 (2003)
104. W.N. Shafarman, J. Zhu, Thin Solid Films **362**, 473 (2000)
105. J.R. Tuttle, D.S. Albin, R. Noufi, Sol. Cells **30**, 21 (1991)
106. R. Klenk, T. Walter, H.W. Schock, D. Cahen, Adv. Mater. **5**, 114 (1993)
107. W.S. Chen, J.M. Stewart, B.J. Stanbery, W.E. Devaney, R.A. Mickelsen, in *19th Photovolt. Spec. Conf. (PVSC)*, p. 1445 (1987)
108. T. Wada, N. Kohara, T. Negami, M. Nishitani, J. Mater. Res. **12**, 1433 (1997)
109. J. Kessler, J. Schöldström, L. Stolt, in *28th IEEE Photovolt. Spec. Conf. (PVSC)*, p. 509 (2000)
110. J. Kessler, D. Schmid, S. Zweigart, H. Dittrich, H.W. Schock, in *12th Eur. PV Sol. Energy Conf.*, p. 648 (1994)
111. S. Nishiwaki, T. Satoh, S. Hayashi, Y. Hashimoto, S. Shimakawa, T. Negami, T. Wada, Sol. Energy Mater. Sol. Cells **67**, 217 (2001)
112. P. Jackson, D. Hariskos, R. Wuerz, W. Wischmann, M. Powalla, Phys. Status Solidi RRL **8**, 219 (2014)
113. D.J. Schroeder, G.D. Berry, A. Rockett, Appl. Phys. Lett. **69**, 4068 (1996)
114. O. Lundberg, J. Lu, A. Rockett, M. Edoff, L. Stolt, J. Phys. Chem. Solids. **64**, 1499 (2003)
115. L. Gartsman, V. Chernyak, D. Lyahovitskaya, V. Cahen, V. Didik, R. Kozlovsky, E. Malkovich, V.U. Skoryatina, J. Appl. Phys. **82**, 4282 (1997)
116. C. Lei, A. Rockett, I.M. Robertson, W.N. Shafarman, M. Beck, J. Appl. Phys. **100**, 073518 (2006)
117. T. Mise, T. Nakada, Sol. Energy Mater. Sol. Cells. **93**, 1000 (2009)
118. S. Ishizuka, A. Yamada, P.J. Fons, H. Shibata, S. Niki, Prog. Photovolt. Res. Appl. **22**, 821 (2014)
119. K.H. Kim, K.H. Yoon, J.H. Yun, B.T. Ahn, Electrochem. Solid-State Lett. **9**, A382 (2006)
120. S. Chaisitsak, A. Yamada, M. Konagai, Jpn. J. Appl. Phys. **41**, 507 (2002)
121. U.P. Singh, S.P. Patra, Int. J. Photoenergy **2010**, 1 (2010)
122. Y.E. Romanyuk, H. Hagendorfer, P. Stücheli, P. Fuchs, A.R. Uhl, C.M. Sutter-Fella, P.P. Grand, Adv. Funct. Mater. **25**, 12 (2015)
123. T. Feurer, P. Reinhard, E. Avancini, B. Bissig, J. Löckinger, P. Fuchs, S. Buecheler, Prog. Photovolt. Res. Appl. **25**, 645 (2017)
124. S. Niki, M. Contreras, I. Repins, M. Powalla, K. Kushiya, S. Ishizuka, K. Matsubara, Prog. Photovolt. Res. Appl. **18**, 453 (2010)
125. R. Kamada, T. Yagioka, S. Adachi, A. Handa, K.F. Tai, T. Kato, H. Sugimoto, in *2016 IEEE 43rd Photovolt. Spec. Conf. (PVSC)*, p. 1287 (2016)
126. K.W. Mitchell, H.I. Liu, in *12th IEEE Photovolt. Spec. Conf. (PVSC)*, p. 1461 (1988)
127. A. Chirilă, P. Reinhard, F. Pianezzi, P. Bloesch, A.R. Uhl, C. Fella, D. Jaeger, Nat. Mater. **12**, 1107 (2013)
128. H.K. Song, J.K. Jeong, H.J. Kim, S.K. Kim, K.H. Yoon, Thin Solid Films **435**, 186 (2003)
129. T. Nakabayashi, T. Miyazawa, Y. Hashimoto, K. Ito, Sol. Energy Mater. Sol. Cells **49**, 375 (1997)
130. J.P. Bäcker, S.S. Schmidt, H. Rodriguez-Alvarez, C. Wolf, C.A. Kaufmann, M. Hartig, R. Schlatmann, Sol. Energy Mater. Sol. Cells **162**, 120 (2017)
131. H.K. Song, S.G. Kim, H.J. Kim, S.K. Kim, K.W. Kang, J.C. Lee, K.H. Yoon, Sol. Energy Mater. Sol. Cells **75**, 145 (2003)
132. H. Park, S.C. Kim, S.H. Lee, J. Koo, S.H. Lee, C.W. Jeon, W.K. Kim, Thin Solid Films **519**, 7245 (2011)
133. S.S. Schmidt, C. Wolf, H. Rodriguez-Alvarez, J.P. Bäcker, C.A. Kaufmann, S. Merdes, C. Köble, Prog. Photovolt. Res. Appl. **25**, 341 (2017)
134. T.T. Wu, J.H. Huang, F. Hu, C.H. Chang, W.L. Liu, T.H. Wang, Y.L. Chueh, Nano Energy **10**, 28 (2014)
135. G.S. Chen, J.C. Yang, Y.C. Chan, L.C. Yang, W. Huang, Sol. Energy Mater. Sol. Cells **93**, 1351 (2009)
136. N. Kohara, S. Nishiwaki, Y. Hashimoto, T.T. Negami Wada, Sol. Energy Mater. Sol. Cells **67**, 209 (2001)
137. K.J. Hsiao, J.D. Liu, H.H. Hsieh, T.S. Jiang, Phys. Chem. Chem. Phys. **15**, 18174 (2013)
138. R. Usui, T. Tomizawa, T. Okato and H. Odaka, in *38th IEEE Photovolt. Spec. Conf. (PVSC)*, p. 3109 (2012)
139. T. Wada, N. Kohara, T. Negami, M. Nishitani, Jpn J. Appl. Phys. **35**, L1253 (1996)
140. D. Abou-Ras, G. Kostorz, D. Bremaud, M. Kälin, F.V. Kurdesau, A.N. Tiwari, M. Döbeli, Thin Solid Films **480**, 433 (2005)
141. T. Klinkert, B. Theys, G. Patriarche, M. Jubault, F. Donsanti, J.F. Guillemoles, D. Lincot, J. Chem. Phys. **145**, 154702 (2016)
142. T. Wada, N. Kohara, S. Nishiwaki, T. Negami, Thin Solid Films **387**, 118 (2001)
143. W. Liu, Y. Sun, W. Li, C.J. Li, F.Y. Li, J.G. Tian, Appl. Phys. A **88**, 653 (2007)
144. Y.C. Wang, H.P.D. Shieh, Appl. Phys. Lett. **105**, 073901 (2014)
145. H.R. Hsu, S.C. Hsu, Y.S. Liu, Appl. Phys. Lett. **100**, 233903 (2012)
146. M. Marudachalam, H. Hichri, R. Klenk, R.W. Birkmire, W.N.J.M. Shafarman Schultz, Appl. Phys. Lett. **67**, 3978 (1995)
147. S.K. Lee, J.K. Sim, N.S. Kissinger, I.S. Song, J.S. Kim, B.J. Baek, C.R. Lee, J. Alloys Compd. **633**, 31 (2015)
148. Y.C. Wang, H.P.D. Shieh, Appl. Phys. Lett. **103**, 153502 (2013)
149. M.S. Park, S.J. Sung, D.H. Kim, J. Nanosci. Nanotechnol. **15**, 2490 (2015)
150. S.Y. Hsiao, P.C. Yang, H.C. Ni, K.Y. Yen, C.H. Chiu, P.S. Lin, F.W. Jih, J. Electrochem. Soc. **159**, H378 (2012)
151. G. Li, W. Liu, Y. Liu, S. Lin, X. Li, Y. Zhang, Y. Sun, Semicond. Sci. Technol. **30**, 105012 (2015)
152. S.M. Youn, J.H. Kim, C. Jeong, J. Nanosci. Nanotechnol. **16**, 5003 (2016)
153. P. Schöppe, C.S. Schnohr, M. Oertel, A. Kusch, A. Johannes, S. Eckner, C. Ronning, Appl. Phys. Lett. **106**, 013909 (2015)
154. H. Azimi, Y. Hou, C.J. Brabec, Energy Environ. Sci. **7**, 1829 (2014)
155. S.N. Sharma, P. Chawla, A.K. Srivastava, Physica E **80**, 101 (2016)
156. S.N. Chawla, S.S. Sharma, J. Solid State Chem. **219**, 9 (2014)
157. C. Eberspacher, C. Fredric, K. Pauls, J. Serra, Thin Solid Films **387**, 18 (2001)
158. J. Tang, S. Hinds, S.O. Kelley, E.H. Sargent, Chem. Mater. **20**, 6906 (2008)
159. P. Chawla, S.S.N. Singh Sharma, Belstein J. Nanotechnol. **5**, 1235 (2014)
160. K.H. Ahn, J.H. Kim, K.H.Y. Yun, J. Appl. Phys. **105**, 113533 (2009)
161. D.L. Schulz, C.J. Curtis, R.A. Flitton, H. Wiesner, J. Keane, R.J. Matson, M. Kim, P.A. Parilla, R. Noufi, D.S. Ginley, J. Electron. Mater. **27**, 433 (1998)
162. M. Guo, G.M. Ford, R. Agrawal, H.W. Hillhouse, Prog. Photovolt. Res. Appl. **155**, 64 (2013)
163. P. Chawla, M. Ahamed, N. Vijayan, S.N. Sharma, in *Springer Proceedings in Physics, Recent Trends in Materials and Devices*, p. 489 (2016)

164. M. Ahamed, P. Chawla, S.N. Sharma, *Springer Proceedings in Physics, Recent Trends in Materials and Devices*, p. 483 (2016)
165. C. Jiang, J. Lee, D.V. Talapin, J. Am. Chem. Soc. **134**, 5010 (2012)
166. M. Kaelin, D. Rudmann, F. Kurdesau, T. Meyer, H. Zogg, A.N. Tiwari, Thin Solid Films **431**, 58 (2003)
167. M. Kaelin, D. Rudmann, A.N. Tiwari, Sol. Energy **77**, 749 (2004)
168. V.K. Kapur, A. Bansal, P. Le, O.I. Asensio, Thin Solid Films **431**, 53 (2003)
169. G. Brown, P. Stone, J. Woodruff, B. Cardozo, D. Jackrel, in *38th IEEE Photovolt. Spec. Conf. (PVSC)*, p. 3230 (2012)
170. T.K. Todorov, D.B. Mitzi, Eur. J. Inorg. Chem. **2010**, 17 (2010)
171. R.N. Bhattacharya, J. Electrochem. Soc. **130**, 2040 (1983)
172. R.N. Bhattacharya, Sol. Energy Mater. Sol. Cells **113**, 96 (2013)
173. J. Bi, J. Ao, Q. Gao, Z. Zhang, G. Sun, Q. He, Z. Zhou, Y. Sun, Y. Zhang, ACS Appl. Mater. Interfaces **9**, 18682 (2017)
174. R.N. Bhattacharya, J.F. Hiltner, W. Batchelor, M.A. Contreras, R.N. Noufi, J.R. Sites, Thin Solid Films **361**, 396 (2000)
175. F. Liu, C. Huang, Y. Lai, Z. Zhang, J. Li, Y. Liu, J. Alloys Compd. **509**, L129 (2011)
176. A. Duchatelet, T. Sidali, N. Loones, G. Savidand, E. Chassaing, D. Lincot, Sol. Energy Mater. Sol. Cells **119**, 241 (2013)
177. J. Yang, C. Huang, L. Jiang, F. Liu, Y. Lai, J. Li, Y. Liu, Electrochim. Acta **142**, 208 (2014)
178. M. Steichen, M. Thomassey, S. Siebentritt, P.J. Dale, Phys. Chem. Chem. Phys. **13**, 4292 (2011)
179. J.C. Malaquias, D.M. Berg, J. Sendler, M. Steichen, N. Valle, P.J. Dale, Thin Solid Films **582**, 2 (2015)
180. A.B. Rohom, P.U. Londhe, N.B. Chaure, J. Electrochem. Soc. **165**, H3051 (2018)
181. O.A. Oviedo, L. Reinaudi, S.G. García, E.P.M. Leiva, *Underpotential deposition*, 1st edn. (Springer, Switzerland, 2016), pp. 1–13
182. V.S. Saji, I.H. Choi, C.W. Lee, Sol. Energy **85**, 2666 (2011)
183. F. Kang, J.P. Ao, G.Z. Sun, Q. He, Y. Sun, Semicond. Sci. Technol. **24**, 075015 (2009)
184. N.D. Sang, P.H. Quang, L.T. Tu, D.T.B. Hop, Bull. Mater. Sci. **36**, 735 (2013)
185. M. Ganchev, J. Kois, M. Kaelin, S. Bereznev, E. Tzvetkova, O. Volobujeva, N. Stratieva, A. Tiwari, Thin Solid Films **511**, 325 (2006)
186. T.K. Todorov, O. Gunawan, T. Gokmen, D.B. Mitzi, Prog. Photovolt. Res. Appl. **21**, 82 (2013)
187. C. Ahn, J.H. Kim, J. Yun, S. Gwak, B. Jeong, K.Y. Ryu, J. Phys. Chem. C. **114**, 8108 (2010)
188. M. Kaelin, D. Rudmann, F. Kurdesau, T. Meyer, H. Zogg, A.N. Tiwari, Thin Solid Films **480**, 486 (2005)
189. A.R. Uhl, Y.E. Romanyuk, A.N. Tiwari, Thin Solid Films **519**, 7259 (2011)
190. A.R. Uhl, C. Fella, A. Chirilă, M.R. Kaelin, L. Karvonen, A. Weidenkaff, C.N. Borca, D. Grolimund, Y.E. Romanyuk, A.N. Tiwari, Prog. Photovolt. Res. Appl. **20**, 526 (2012)
191. S.J. Park, J.W. Cho, J.K. Lee, K. Shin, J. Kim, B.K. Min, Prog. Photovolt. Res. Appl. **22**, 122 (2014)
192. M. Krunks, O. Kijatkina, H. Rebane, I. Oja, V. Mikli, A. Mere, Thin Solid Films **403**, 71 (2002)
193. M.A. Hossain, Z. Tianliang, L.K. Keat, L. Xianglin, R.R. Prabhakar, S.K. Batabyal, S.G. Mhaisalkar, L.H. Wong, J. Mater. Chem. A. **3**, 4147 (2015)
194. W. Septina, M. Kurihara, S. Ikeda, Y. Nakajima, T. Hirano, Y. Kawasaki, T. Harada, M. Matsumura, ACS Appl. Mater. Interfaces **7**, 6472 (2015)
195. M. Lazell, M. Brien, D.J. Otway, J.H. Park, J. Chem. Soc. Dalt. Trans. **24**, 4479 (2000)
196. W. Hirpo, S. Dhingra, A.C. Sutorik, M.G. Kanatzidis, J. Am. Chem. Soc. **115**, 1597 (1993)
197. J.D. Harris, K.K. Banger, D.A. Scheiman, M.A. Smith, M.H.C. Jin, A.F. Hepp, Mater. Sci. Eng. B **98**, 150 (2003)
198. M.H. Jin, K.K. Banger, C.V.. Kelly, J.H. Scofield, J.S. Mcnatt, J.E. Dickman, A.F. Hepp, in *19th Eur. Photovolt. Sol. Energy Conf.* (2004)
199. B. Bob, B. Lei, C.H. Chung, W. Yang, W.C. Hsu, H.S. Duan, W.W.J. Hou, S.H. Li, V. Yang, Adv. Energy Mater. **2**, 504 (2012)
200. D.B. Mitzi, Adv. Mater. **21**, 3141 (2009)
201. H. Zhou, C.J. Hsu, W.C. Hsu, H.S. Duan, C.H. Chung, W. Yang, Y. Yang, Adv. Energy Mater. **3**, 328 (2013)
202. W. Zhao, Y. Cui, D. Pan, Energy Technol. **1**, 131 (2013)
203. C. Broussillou, C. Viscogliosi, A. Rogee, S. Angle, P.P. Grand, S. Bodnar, C. Debauche, J.L. Allary, B. Bertrand, C. Guillou, L. Parissi, S. Coletti, in *IEEE 42nd Photovolt. Spec. Conf. (PVSC)*, vol. 1 (2015)
204. C. Insignares-Cuello, F. Oliva, M. Neuschitzer, X. Fontané, C. Broussillou, T.G. de Monsabert, E. Saucedo, C. Ruiz, A. Pérez-Rodríguez, V. Izquierdo-Roca, Sol. Energy Mater. Sol. Cells **143**, 212 (2015)
205. Y. Yang, G. Wang, W. Zhao, Q. Tian, L. Huang, D. Pan, ACS Appl Mater. Interfaces **7**, 460 (2014)
206. Aksu, S. Pethe, A. Kleiman-Shwarsctein, S. Kundu, M. Pinarbasi, in *38th IEEE Photovolt. Spec. Conf. (PVSC)*, p. 003092 (2012)
207. J. Bi, L. Yao, J. Ao, S. Gao, G. Sun, Q. He, Z. Zhou, Y. Sun, Y. Zhang, J. Power Sources **326**, 211 (2016)
208. F. Kang, J. Ao, G. Sun, Q. He, Y. Sun, J. Alloys Compd. **478**, L25 (2009)
209. https://www.ascentsolar.com/. Accessed 27 Aug 2019
210. https://flisom.com/products/. Accessed 27 Aug 2019
211. https://www.globalsolar.com/. Accessed 27 Aug 2019
212. https://solibro-solar.com/en/. Accessed 27 Aug 2019
213. https://www.manz.com/markets/solar/cigs-fab/success-factors/. Accessed 27 Aug 2019
214. https://miasole.com/products/. Accessed 27 Aug 2019
215. https://www.solarfrontier.com/eng/solutions/products/index.html. Accessed 27 Aug 2019
216. https://www.avancis.de/en/. Accessed 27 Aug 2019
217. https://www.ips.co.kr/eng_main/sub3-6.php. Accessed 27 Aug 2019
218. https://www.stion.com/products/. Accessed 27 Aug 2019
219. https://midsummer.se/applications. Accessed 27 Aug 2019
220. https://www.hulket.com/. Accessed 27 Aug 2019
221. https://solopower.com/products/. Accessed 27 Aug 2019
222. R. Caballero, C. Guillén, Thin Solid Films **403**, 107 (2002)
223. S. Repins, J. Glynn, T.J. Duenow, W.K. Coutts, M.A. Metzger, *Contreras Proc. SPIE 7409, 74090M–14* (2009)
224. W. Liu, D.B. Mitzi, M. Yuan, A.J. Kellock, S.J.O. Chey Gunawan, Chem. Mater. **22**, 1010 (2010)

Publisher's Note Springer Nature remains neutral with regard to jurisdictional claims in published maps and institutional affiliations.